

DETECTION OF ELEMENTS AT ALL THREE *R*-PROCESS PEAKS IN THE METAL-POOR STAR HD 160617^{1,2,3}

IAN U. ROEDERER⁴ AND JAMES E. LAWLER⁵

Published in the Astrophysical Journal

ABSTRACT

We report the first detection of elements at all three *r*-process peaks in the metal-poor halo star HD 160617. These elements include arsenic and selenium, which have not been detected previously in halo stars, and the elements tellurium, osmium, iridium, and platinum, which have been detected previously. Absorption lines of these elements are found in archive observations made with the Space Telescope Imaging Spectrograph onboard the *Hubble Space Telescope*. We present up-to-date absolute atomic transition probabilities and complete line component patterns for these elements. Additional archival spectra of this star from several ground-based instruments allow us to derive abundances or upper limits of 45 elements in HD 160617, including 27 elements produced by neutron-capture reactions. The average abundances of the elements at the three *r*-process peaks are similar to the predicted solar system *r*-process residuals when scaled to the abundances in the rare earth element domain. This result for arsenic and selenium may be surprising in light of predictions that the production of the lightest *r*-process elements generally should be decoupled from the heavier *r*-process elements.

Subject headings: atomic data — nuclear reactions, nucleosynthesis, abundances — stars: abundances — stars: individual (HD 160617) — stars: Population II

1. INTRODUCTION

Understanding the origin of the elements is one of the major challenges of modern astrophysics. Heavy elements, here considered to be those more massive than the iron-group, are primarily produced by neutron-capture (*n*-capture) reactions. The heavy elements in the solar system (S.S.) were produced mainly by two kinds of *n*-capture reactions, those slow (the *s*-process) or rapid (the *r*-process) relative to the average β -decay timescales of nuclei along the reaction chain. The nuclear structure of atoms and the conditions at the time of nucleosynthesis determine the relative abundance patterns. The abundance patterns can be interpreted through the lens of experimental or theoretical properties of atomic nuclei to infer the conditions present in the supernovae, merging neutron stars, or red giant stars where these elements were forged.

Large energy gaps to the next highest nuclear energy level occur in nuclei with 50, 82, and 126 neutrons. Nuclei with these “closed” nuclear shells are especially stable and resist further *n*-capture, so they are produced

in greater abundance during *n*-capture reactions. The *s*-process path closely follows the valley of β -stability, whereas the *r*-process blazes a path through neutron-rich nuclei. The *r*-process encounters the closed shells in nuclei of lower proton number, Z , than the *s*-process does, so the abundance peaks of the *r*-process are shifted to lower-mass atoms relative to the *s*-process peaks.

Most elements at the three *s*-process peaks are readily identified in optical spectra obtained from ground-based instruments (e.g., Merrill 1926; St. John & Moore 1928; Aller & Greenstein 1960; Wallerstein et al. 1963; Van Eck et al. 2001). These elements include rubidium, strontium, yttrium, and zirconium ($37 \leq Z \leq 40$) at the first *s*-process peak; barium, lanthanum, cerium, praseodymium, and neodymium ($56 \leq Z \leq 60$) at the second *s*-process peak; and lead and bismuth ($82 \leq Z \leq 83$) at the third *s*-process peak. In contrast, elements at the third *r*-process peak—osmium, iridium, and platinum ($76 \leq Z \leq 78$)—remained undetected in halo stars until the Goddard High Resolution Spectrograph (GHRS) onboard the *Hubble Space Telescope* (*HST*) revealed the ultraviolet (UV) spectra of late-type stars in high spectral resolution (Cowan et al. 1996; Sneden et al. 1998).⁶ Subsequent investigations using the successor to the GHRS, the Space Telescope Imaging Spectrograph (STIS), continue to offer the only reliable window to detect these third *r*-process peak elements (Cowan et al. 2002, 2005; Sneden et al. 2003; Roederer et al. 2009, 2010a, 2012b; Barbuy et al. 2011). Only one element at the second *r*-process peak, tellurium ($Z = 52$), was recently detected in three halo stars by

¹ Some of the data presented in this paper were obtained from the Multimission Archive at the Space Telescope Science Institute (MAST). STScI is operated by the Association of Universities for Research in Astronomy, Inc., under NASA contract NAS5-26555. These data are associated with Program GO-8197.

² Based on data obtained from the European Southern Observatory (ESO) Science Archive Facility. These data are associated with Programs 65.L-0507 and 82.B-0610.

³ This research has made use of the Keck Observatory Archive (KOA), which is operated by the W.M. Keck Observatory and the NASA Exoplanet Science Institute (NExScI), under contract with the National Aeronautics and Space Administration. These data are associated with Program H6aH (P.I. Boesgaard).

⁴ Carnegie Observatories, Pasadena, CA 91101, USA; iur@obs.carnegiescience.edu

⁵ Department of Physics, University of Wisconsin, Madison, WI 53706, USA; jelawler@wisc.edu

⁶ Numerous heavy elements, including those at the third *r*-process peak, have long been recognized in the stratified atmospheres of chemically peculiar stars; e.g., Morgan (1933) or Dworetsky (1969). We do not regard these stars as useful for interpreting the nucleosynthetic record, however, so we shall not discuss them further.

Roederer et al. (2012a).

The need for UV access can be explained using a combination of principles from astrophysics, nuclear physics, statistical mechanics, and atomic physics. Here we focus on photospheric temperatures typical for F, G, and K stars. Many of the useful visible and UV lines of iron-group atoms and ions have excitation potentials (E.P.) of ~ 1 eV or more. Even the most abundant lighter n -capture elements tend to have abundances several orders of magnitude below those of iron-group elements. This simple fact eliminates the utility of atomic lines connecting highly excited levels of n -capture elements. It necessitates the use of resonance lines (E.P. = 0) or lines connected to low metastable levels if such levels exist in the atom or ion of interest. A simple consideration of Boltzmann factors reveals the ground and low metastable levels tend to serve as the major population reservoirs for both neutral and singly ionized atoms in a typical photosphere. Depending on the ionization potential (I.P.) of the neutral atom, either the neutral or singly ionized specie is dominant in F, G, and K stars.

Consider n -capture elements near and at the right edge of the periodic table. Rare gases at the right edge (krypton, $Z = 36$, and xenon, $Z = 54$) have deeply bound valence electrons due to their closed p-shells and a huge gap between the ground and lowest excited levels. The atomic structure of rare gases prohibits any photospheric abundance observations even on the strongly dominant neutral ionization stage, whose resonance lines lie below 1500 \AA (e.g., Morton 2000). The elements selenium ($Z = 34$) and bromine ($Z = 35$), adjacent to the rare gas krypton, as well as tellurium and iodine ($Z = 53$), adjacent to the rare gas xenon, have partially filled p-shells. These have some similarities to the rare gases. There are gaps of $\sim 48,000 \text{ cm}^{-1}$ and $67,000 \text{ cm}^{-1}$, respectively, between levels in the ground $4p^n$ configurations and the lowest opposite parity $4p^{n-1} 5s$ configurations of atomic selenium and bromine. Even larger gaps exist in the singly charged ion of each element. The gaps between the ground $5p^n$ configurations and lowest opposite parity $5p^{n-1} 6s$ configurations of tellurium and iodine are somewhat smaller, but still greater than $44,000 \text{ cm}^{-1}$. Only UV lines with low E.P. values are even potentially useful for these elements.

Transition elements, such as osmium, iridium, and platinum, with d-shell valence electrons tend to have lower I.P. values than elements with open p-shells. For many transition elements, the singly-charged ion tends to be the dominant ionization stage. Spectral lines with low E.P. values almost always tend to occur at shorter wavelengths when one (or more) electron(s) is removed from an atom. As a result UV observations are needed for abundance studies on many transition elements.

The rare earth elements lanthanum through lutetium, $57 \leq Z \leq 71$, with f-shell valence electrons are important exceptions. Although the rare earth elements exist almost entirely as singly-ionized species, there are a great many visible transitions with low E.P. values due to the open f-shells and interleaving low-lying 4f, 5p, and 6s orbitals. Their accessibility to ground-based astronomy provides a great opportunity for detailed studies of rare earth abundances (e.g., Sneden et al. 2009). The fact that rare earths are accessible to ground based astronomy

provides some motivation for extensive lab work on these elements (e.g., Lawler et al. 2009). Alkaline earth elements, such as strontium ($Z = 38$) and barium ($Z = 56$), with two valence s-shell electrons are also accessible to ground-based observations, even though they exist primarily as ionized species in typical photospheres.

Elements at the r -process peaks are critical to understanding r -process nucleosynthesis. These serve as key normalization points to constrain the conditions that produce a successful r -process (Kratz et al. 1993). Experimental data are available for only a limited number of short-lived nuclei along the r -process path (Dillmann et al. 2003; Baruah et al. 2008). The Facility for Rare Isotope Beams, under construction at Michigan State University, and similar facilities in other countries will alleviate this shortage of r -process nuclear data in the future. Nuclei at the so-called “waiting-points” are the parent isobars of elements at the r -process peaks, including selenium and tellurium. Yet, until now, the only secure measurements of their abundances in environments suitable for inferring the r -process abundance distribution have come from the S.S. r -process residuals. This method of computing these residuals assumes that the r -process produced some fraction of all heavy isotopes in the S.S. except those attributed to s -process nucleosynthesis or inaccessible to the r -process (e.g., Seeger et al. 1965; Cameron 1982; Käppeler et al. 1989). Light n -capture nuclei may have a variety of origins besides the s - and r -processes (e.g., α -rich freeze-out from nuclear statistical equilibrium; Woosley & Hoffman 1992). Since the assumptions underlying the S.S. r -process residual distribution for the light nuclei are tenuous, detection of these elements in r -process material beyond the S.S. is greatly desired.

Here, we report the detection of two light n -capture elements, arsenic ($Z = 33$) and selenium in an archive STIS UV spectrum of the bright, metal-poor subgiant HD 160617. We also detect elements at the second and third r -process peaks in HD 160617. We supplement these data with ground-based archive spectra to form a more complete estimate of the distribution of the heavy elements in HD 160617. Since many of these transitions are rarely used for abundance analyses, we review the atomic physics literature and make recommendations for the best available $\log(gf)$ values. We also present line component patterns that account for the hyperfine splitting (hfs) structure present in some of these lines.

Throughout this work we use the standard definitions of elemental abundances and ratios. For element X, the logarithmic abundance is defined as the number of atoms of element X per 10^{12} hydrogen atoms, $\log \epsilon(X) \equiv \log_{10}(N_X/N_H) + 12.0$. For elements X and Y, the logarithmic abundance ratio relative to the solar ratio of X and Y is defined as $[X/Y] \equiv \log_{10}(N_X/N_Y) - \log_{10}(N_X/N_Y)_\odot$. Abundances or ratios denoted with the ionization state indicate the total elemental abundance as derived from that particular ionization state after ionization corrections have been applied, not the number density in that particular state. When reporting relative abundance ratios for a specific element X (e.g., $[X/Fe]$), these ratios are constructed by comparing the total abundance of element X derived from the neutral species with the total iron abundance derived from Fe I and the total abundance of element X derived from the ionized species

with the total iron abundance derived from Fe II.

2. OBSERVATIONS FROM THE ARCHIVES

We use four sets of observations of HD 160617 found in different archives. The UV spectrum of HD 160617 is taken from the Multimission Archive at the Space Telescope Science Institute. These observations were made using STIS (Kimble et al. 1998; Woodgate et al. 1998) onboard *HST*. This spectrum has very high spectral resolution ($R \equiv \lambda/\Delta\lambda = 114,000$) and modest signal-to-noise (S/N) levels ranging from ~ 25 –50 per pixel, but it only covers a limited spectral range in the UV ($1879 < \lambda < 2148 \text{ \AA}$). We use the reduction and coaddition provided by the StarCAT database (Ayres 2010).

We use ground-based optical spectra of HD 160617 from several telescope and instrument combinations. Some spectra were retrieved from the European Southern Observatory (ESO) Science Archive Facility. A spectrum obtained with the Ultraviolet and Visual Echelle Spectrograph (UVES; Dekker et al. 2000) on the Very Large Telescope (VLT) Kueyen at Cerro Paranal, Chile, covers the wavelength range 3055–3870 Å at $R \sim 40,000$ with S/N ranging from 100–400 per pixel. A spectrum obtained with the High Accuracy Radial velocity Planet Searcher (HARPS; Mayor et al. 2003) on the ESO 3.6 m Telescope at La Silla, Chile, covers the wavelength range 3780–6910 Å at $R \sim 115,000$ with S/N ranging from 150–300 per pixel. Another spectrum was retrieved from the Keck Observatory Archive. This spectrum was obtained with the High Resolution Echelle Spectrometer (HIRES; Vogt et al. 1994) on the Keck I Telescope at Mauna Kea, Hawai'i. It covers the wavelength range 4395–6770 Å at $R \sim 49,000$ with S/N ranging from 130–300 per pixel. These spectra were reduced and extracted using the standard instrument pipelines before being downloaded, and final processing was performed within the IRAF environment.

2.1. Comparing Spectra Using Equivalent Width Measurements

The different optical spectra of HD 160617 overlap considerably in wavelength coverage. To assess their reliability, we compare the equivalent widths (EW) of lines in common. We measure the EWs using a semi-automatic routine that fits Voigt absorption line profiles to continuum-normalized spectra. We compare the EWs of species of lighter elements whose composition is not expected to be dominated by isotopes with hfs, which could affect the line profiles. These include Mg I, Si I, Ca I, Ti I and II, Cr I and II, Fe I and II, Ni I, and Zn I. We find good internal agreement between the HARPS and HIRES spectra ($\langle\Delta\rangle = +0.9 \pm 0.12 \text{ m\AA}$, $\sigma = 1.6 \text{ m\AA}$, 174 lines). The HARPS and UVES spectra have relatively little overlap, but even there the agreement is reassuring ($\langle\Delta\rangle = -1.0 \pm 1.6 \text{ m\AA}$, $\sigma = 1.6 \text{ m\AA}$, 5 lines). This suggests that systematic differences are not apparent at a level greater than 1 mÅ, so mixing abundances derived from different spectra should not introduce any significant bias into the results.

The HARPS and HIRES spectra have comparable S/N levels, though the HARPS spectrum is of considerably higher spectral resolution. The HIRES spectrum contains a few small order gaps redward of 5050 Å, and the

HARPS spectrum contains one 35 Å gap between the detectors at 5305 Å. Except when a line falls in this gap or appears distorted, we prefer the abundances derived from the HARPS spectrum because of the superior spectral resolution.

3. ATOMIC DATA

We survey the literature on UV lines rarely used in abundance analyses, compare results from various experimental and theoretical studies, and identify the best available transition probabilities, hfs, and isotope shift (IS) data. Here, we discuss these data in greater detail.

3.1. Copper

Seven lines of Cu II, all connecting metastable lower levels of the 1D and 3D terms in the $3d^94s$ configuration to upper levels of the $3d^94p$ configuration are of interest in this study. Due to the size of the spin-orbit splitting compared to term separations, both the upper and lower levels are best described by intermediate coupling schemes rather than by the LS scheme. In order of increasing energy, the LS terms of the upper configuration include $^3P^o$, $^3F^o$, $^1F^o$, $^1D^o$, $^3D^o$, and $^1P^o$, but levels with a common J in these terms are mixed. Level assignments for some levels in the compilation by Sugar & Musgrove (1990) are not consistent with level assignments given by Kono & Hattori (1982). Leading percentages given by Donnelly et al. (1999) are illustrative of the difficulty, for example the $3d^94p \ ^1D_2^o$ level (as assigned by Sugar & Musgrove) was found to be 43% $3d^94p \ ^3F_2^o$, 24% $3d^94p \ ^1D_2^o$, and 19% $3d^94p \ ^3D_2^o$. With intermediate coupling, only the parity and J selection rules for dipole transitions are consistently very strong. There has been extensive theoretical and experimental work on the $3d^94s$ – $3d^94p$ transition probabilities, but unfortunately there is significant scatter in the published results. Our preferred transition probabilities in Table 1 are based on experimental branching fractions from Kono & Hattori and laser induced fluorescence (LIF) radiative lifetime measurements by Pinnington et al. (1997) wherever available. Brief line-by-line discussions are appropriate in the case of Cu II.

The line at 2135 Å connects the upper $3d^94p \ ^3F_4^o$ level to the lower $3d^94s \ ^3D_3$ level with a branching fraction of 1.0 due to the J selection rule. Pinnington et al. (1997) reported a LIF measurement of $2.18 \pm 0.04 \text{ ns}$ for the upper level lifetime. Even if their $\sim 2\%$ lifetime uncertainty is somewhat optimistic, the transition probability of the 2135 Å line is very well known. The line at 2126 Å connects the upper $3d^94p \ ^3F_2^o$ level to the lower $3d^94s \ ^3D_2$ level with a branching fraction of 0.403 (Kono & Hattori 1982). This branching fraction has been confirmed to within 2% by Crespo López-Urrutía et al. (1994). Unfortunately no LIF lifetime measurement is available for the upper level. Inspection of Table 1 in Pinnington et al. reveals that theoretical lifetimes by Theodosiou (1986) are generally in good agreement with the LIF measurements, and we combine the above experimental branching fraction with Theodosiou's 2.34 ns theoretical lifetime to determine the transition probability for the 2126 Å line in Table 1. No uncertainty is given in Table 1, but it is likely smaller than $\pm 15\%$.

The line at 2112 Å connects the upper $3d^94p \ ^1P_1^o$ to the

TABLE 1
TRANSITION PROBABILITIES FOR CU II LINES OF INTEREST

Wavelength ^a (Å)	E _{upper} (cm ⁻¹)	J _{upper}	E _{lower} (cm ⁻¹)	J _{lower}	A (10 ⁶ s ⁻¹)	log(gf)
2135.9808	68730.893	4	21928.754	3	459±8	+0.45
2126.0443	69867.983	2	22847.131	2	172	-0.23
2112.1003	73595.813	1	26264.568	2	384	-0.11
2104.7963	71493.853	2	23998.381	1	92±7	-0.51
2054.9790	71493.853	2	22847.131	2	162±12	-0.29
2037.1270	71920.102	3	22847.131	2	134±10	-0.23
1979.9565	73353.292	2	22847.131	2	88±5	-0.59

^a Air wavelengths are given for $\lambda > 2000$ Å and vacuum values below.

lower $3d^9 4s \ ^1D_2$ level, and this is the most problematic case of Table 1. The difficulty is due to the strong 1358 Å line from the upper $^1P_1^o$ level to the ground $3d^{10} \ ^1S_0$ level. There is no direct experimental measurement of the 1358 Å branching fraction, but the short upper level lifetime of 1.34 ± 0.22 ns from Pinnington et al. (1997) and elementary theoretical considerations indicate that the line has a significant branching fraction. Brown et al. (2009) used the beam foil technique to confirm the short upper level lifetime and have recommended a branching fraction of 0.45 for the 1358 Å line based on earlier theoretical work. By combining this branching fraction for the 1358 Å line, measurements of the branching ratios of other emission lines from the upper $^1P_1^o$ level by Kono & Hattori (1982), and the LIF lifetime measurement by Pinnington et al., we compute a transition probability for the 2112 Å line given in Table 1. No uncertainty can be given for the 2112 Å transition probability without additional experimental work.

The next two lines in Table 1 at 2104 Å and 2054 Å are both from the upper $3d^9 4p \ ^1D_2^o$ level (assigned as $^3D_2^o$ by Kono & Hattori 1982) to the lower $3d^9 4s \ ^3D_1$ and 3D_2 levels with measured branching fractions of 0.229 and 0.402 respectively. A LIF lifetime measurement of 2.48 ± 0.05 ns by Pinnington et al. (1997) is available for the upper level. Uncertainties on the transition probabilities are from the 2% lifetime uncertainty and from a 7% branching fraction uncertainty for each line. The 2037 Å from the upper $3d^9 4p \ ^3D_3^o$ level (assigned as $^1F_3^o$ by Kono & Hattori) to the lower $3d^9 4s \ ^3D_2$ level also has a measured branching fraction of 0.296 from Kono & Hattori and a LIF lifetime measurement of 2.21 ± 0.04 ns by Pinnington et al. This branching fraction of the 2037 Å line was confirmed to within 2% by Crespo López-Urrutia et al. (1994). The last line in Table 1 at 1979 Å connects the upper $3d^9 4p \ ^3D_2^o$ level (assigned as $^1D_2^o$ by Kono & Hattori) to the lower $3d^9 4s \ ^3D_2$ level with a measured branching fraction of 0.222. The upper level has a LIF lifetime measurement of 2.51 ± 0.09 ns by Pinnington et al. is combined with the branching fraction to determine the transition probability in Table 1.

Energy levels in Table 1 are from the compilation by Sugar & Musgrove (1990) based on interferometric measurements by Reader et al. (1960). Air wavelengths for lines above 2000 Å are from the level energies and index of air (Peck & Reeder 1972).

The Cu II lines of interest are expected to have non-

negligible hfs and IS structure because Cu is an odd Z element with two $I = 3/2$ isotopes. The S.S. isotopic abundances are 69.15% for ^{63}Cu and 30.85% for ^{65}Cu (Böhlke et al. 2005). These isotopes have nearly equal nuclear magnetic dipole moments from the unpaired proton in each nucleus. The only available experimental hfs and IS data for the lines of interest are those reported by Elbel et al. (1963), and unfortunately these are not accurate by modern (laser spectroscopy) standards. Elbel & Hühnermann (1969) later reported some theoretical work on the IS of the $3d^9 4s$ levels. We use the available experimental data on the hfs and IS data from Elbel et al. for the $3d^9 4s$ and $3d^9 4p$ levels to generate complete line component patterns of the strongest Cu II lines of interest. We find that the abundance results for the 2126 Å and 2112 Å lines are changed by less than 0.01 dex when including the effect of hfs. Complete line component patterns for Cu II lines are omitted from this paper with the expectation that more accurate lab data will soon be available for the Cu II lines of interest.

3.2. Zinc

Lines of both Zn I and Zn II are of interest in this study. The multiplet of Zn I near 4750 Å connecting the lower $4s 4p \ ^3P^o$ term to the upper $4s 5s \ ^3S_1$ level is a nearly pure Russell-Saunders (LS) multiplet. Early experimental branching fractions (Schuttevaer & Smit 1943) as well as theoretical considerations are consistent with the nearly pure LS character. For the lower $4s 4p \ ^3P^o$ term the relatively small fine structure splitting, $< 600 \text{ cm}^{-1}$, compared to the separation, $> 14000 \text{ cm}^{-1}$, from other levels which can mix is indicative of a nearly pure LS term. Several independent measurements and calculations of the upper level lifetime, including the preferred LIF measurement of $8.0(4)$ ns (Kerkhoff et al. 1980), are consistent to $\pm 10\%$. The selected transition probabilities in Table 2 are from Kerkhoff et al. The second multiplet of Zn I near 3300 Å connecting the same lower $4s 4p \ ^3P^o$ term to the upper $4s 4d \ ^3D$ term is also a nearly pure LS multiplet. Similar to the above case the early experimental branching fractions (Schuttevaer & Smit 1943) as well as theoretical considerations are consistent with the nearly pure LS character. For the upper $4s 4d \ ^3D$ term the very small fine structure splitting, $< 10 \text{ cm}^{-1}$ total, compared to the separation, $> 300 \text{ cm}^{-1}$, from other levels which can mix is indicative of a nearly pure LS term. Several independent sets of measurements and calculations of the upper level lifetimes, including two sets of LIF measurements (Kerkhoff et al. 1980; Blagoev et al.

TABLE 2
TRANSITION PROBABILITIES FOR ZN I AND ZN II LINES OF INTEREST

Air wavelength (Å)	E_{upper} (cm^{-1})	J_{upper}	E_{lower} (cm^{-1})	J_{lower}	A (10^6 s^{-1})	$\log(gf)$	Spectrum
4810.5321	53672.240	1	32890.327	2	67 ± 3	-0.15	Zn I
4722.1569	53672.240	1	32501.399	1	43 ± 2	-0.37	Zn I
4680.1362	53672.240	1	32311.319	0	15.0 ± 0.8	-0.85	Zn I
3345.9353	62768.747	1	32890.327	2	4 ± 0.2	-1.66 ^a	Zn I
3345.5695	62772.014	2	32890.327	2	38 ± 2	-0.51	Zn I
3345.0134	62776.981	3	32890.327	2	156 ± 8	+0.26	Zn I
3302.9394	62768.747	1	32501.399	1	66 ± 3	-0.48	Zn I
3302.5829	62772.014	2	32501.399	1	118 ± 6	-0.02	Zn I
3282.3256	62768.747	1	32311.319	0	90 ± 5	-0.36	Zn I
3075.8970	32501.399	1	0.000	0	0.0329	-3.85	Zn I
2062.0012	48481.077	0.5	0.000	0.5	400 ± 32	-0.29	Zn II

^a The $\log(gf)$ value has been adjusted by +0.04 dex to correct a truncation in the Einstein A value from Kerkhoff et al. (1980).

2004), are consistent to within $\pm 10\%$ for all three levels of the upper term. The selected results in Table 2 are from Kerkhoff et al. These values agree very well the critical compilation by Reader et al. (1980).

The very weak spin-forbidden line at 3075 Å connects the ground $4s^2 \ ^1S_0$ levels of the neutral atom to the $4s4p \ ^3P_1^o$ level. This weak line is useful in this abundance study due to the relatively high abundance of zinc and due to the ionization balance only slightly favoring the singly ionized specie over the neutral atom. The branching fraction of the 3075 Å line is 1.0; however, the radiative lifetime is too long for standard LIF experimental setups. This is expected because the $4s4p \ ^3P_1^o$ term is nearly pure LS and the $4s4p \ ^1P_1^o$ level is only very slightly mixed with the much higher $4s4p \ ^1P_1^o$ level yielding a radiative lifetime longer than 10 μs . The critical compilation of Reader et al. (1980) included a transition probability with an accuracy B ($\pm 10\%$ or ± 0.04 dex), but recent theoretical values have diverged somewhat from the 1980 compiled result of $\log(gf) = -3.854$. Chen & Cheng (2010) found $\log(gf) = -3.72$. Liu et al. (2006) found -3.78. Chou et al. (1994) found -3.89. For the near future we recommend that the compilation value of $\log(gf) = -3.854$ be used, but with the realization the uncertainty is somewhat larger than 0.04 dex.

Only the 2062.00 Å line of Zn II is included in this study. This line has a branching fraction of 1.0 and connects the ground $4s \ ^2S_{1/2}$ level to the $4p \ ^2P_{1/2}^o$ level. Bergeson & Lawler (1993) measured the upper level lifetime using LIF. More recent theoretical investigations have reproduced their 2.5(2) ns radiative lifetime measurement to within one-half of an error bar (Harrison & Hibbert 2003; Dixit et al. 2008a). The $\log(gf)$ in Table 2 is the value from their LIF experiment.

New lab measurements using Fourier transform spectrometers of both Zn I and Zn II wavenumbers or wavelengths have recently been performed to support studies of possible changes in the fine structure constant during the expansion of the Universe (Gullberg & Litzén 2000; Pickering et al. 2000). Energy levels in Table 2 are from Gullberg & Litzén. The Zn II wavelengths from Pickering et al. are in perfect (0.0001 Å) agreement with those of Gullberg & Litzén. Wavelengths are computed from the energy levels using the index of air (Peck & Reeder 1972).

3.3. Arsenic

Three of the four As I lines of interest in this study are members of a multiplet between the ground $4s^2 4p^3 \ ^4S^o$ term and the excited $4s^2 4p^2 ({}^3P) 5s \ ^4P$ term. The fourth line at 1890 Å is from the metastable $4s^2 4p^3 \ ^2D_{3/2}^o$ level of the ground configuration to the excited $4s^2 4p^2 ({}^1D) 5s \ ^2D_{3/2}$ level. There has been both experimental and theoretical work on the transition probabilities of these 4p–5s lines. Bengtsson et al. (1992a) reported radiative lifetime measurements using LIF on two of the three levels in the $4s^2 4p^2 ({}^3P) 5s \ ^4P$ term, and they used these to normalize experimental branching fractions measured by Lotrian et al. (1980) for the 1972 Å and 1937 Å lines included in Table 3. Russell-Saunders (LS) coupling is fairly good for these low levels of As, and the lines of interest are dominant branches, which minimizes the branching fraction uncertainty. Holmgren (1975) and later Bieron & Migdaek (1992) computed transition probabilities for As I lines of interest and found good agreement with the above experimental results. Holmgren’s theoretical transition probabilities for the 1990 Å and 1890 Å lines are included in Table 3 with experimental results for the other two lines.

Arsenic has one stable isotope with a nuclear spin of $I = 3/2$. Hyperfine patterns for the lines of interest are provided in Table 4, based on extremely accurate hyperfine A and B coefficients for the ground level. These were measured using a radio frequency technique by Pendlebury & Smith (1964), and hyperfine A coefficients for other levels were measured using an optical technique by Bouazza et al. (1987). The vacuum wavelengths and energy levels are from Howard & Andrew (1985).

3.4. Selenium

Three of the four Se I lines of interest in this study are members of a multiplet between the ground $4s^2 4p^4 \ ^3P$ term and the excited $4s^2 4p^3 ({}^4S) 5s \ ^3S_1^o$ level. The fourth line is spin forbidden and thus weak. It connects the ground 3P_2 level to the excited $4s^2 4p^3 ({}^4S) 5s \ ^5S_2^o$ level. After careful review of both older and more recent literature, we conclude that Morton’s (2000) recommendations for wavelengths and transition probabilities of these Se I lines are still up-to-date. Morton chose radiative lifetimes measured using

TABLE 3
TRANSITION PROBABILITIES FOR AS I LINES OF INTEREST

Vacuum wavelength (Å)	E_{upper} (cm^{-1})	J_{upper}	E_{lower} (cm^{-1})	J_{lower}	A (10^6 s^{-1})	$\log(gf)$
1990.3552	60834.954	1.5	10592.666	1.5	220	-0.28
1972.6240	50693.897	0.5	0.000	1.5	202±22	-0.63
1937.5942	51610.393	1.5	0.000	1.5	219±25	-0.31
1890.4286	52898.056	2.5	0.000	1.5	200	-0.19

TABLE 4
HYPERFINE STRUCTURE LINE COMPONENT PATTERNS FOR $^{75}\text{As I}$

Wavenumber (cm^{-1})	λ_{vac} (Å)	F_{upper}	F_{lower}	Component Position (cm^{-1})	Component Position (Å)	Strength
50242.288	1990.3552	3	3	0.01800	-0.000713	0.35000
50242.288	1990.3552	3	2	0.06600	-0.002615	0.08750
50242.288	1990.3552	2	3	-0.05400	0.002139	0.08750

NOTE. — The line component patterns are computed from HFS constants of Pendlebury & Smith (1964) and Bouazza et al. (1987). Center-of-gravity wavenumbers and vacuum wavelengths, λ_{vac} , from Howard & Andrew (1985), are given with component positions relative to those values. Strengths are normalized to sum to 1. Table 4 is available in its entirety via the link to the machine-readable table above.

TABLE 5
TRANSITION PROBABILITIES FOR SE I LINES OF INTEREST

Wavelength ^a (Å)	E_{upper} (cm^{-1})	J_{upper}	E_{lower} (cm^{-1})	J_{lower}	A (10^6 s^{-1})	$\log(gf)$
2074.7841	48182.420	2	0.00	2	1.70±0.10	-2.26
2062.7789	50997.161	1	2534.36	0	33±6	-1.20
2039.8420	50997.161	1	1989.497	1	98±17	-0.74
1960.8935	50997.161	1	0.00	2	213±37	-0.43

^a Air wavelengths are given for $\lambda > 2000 \text{ Å}$ and vacuum values below.

LIF by Bengtsson et al. (1992b,c) for both upper levels and combined these with emission branching fractions from Ubelis & Berzinsh (1986). Morton used energy levels from Morillon & Vergès (1974) with a correction of $+0.23 \text{ cm}^{-1}$ for higher levels recommended by Lindgren & Palenius (1977). These results are summarized in Table 5.

There are 6 naturally-occurring isotopes of selenium found on earth. The isotope shifts are small and can be neglected for our purposes. Only one isotope, ^{77}Se , has non-zero nuclear spin $I = 1/2$. This isotope comprises only 7.6% of natural selenium (Böhlke et al. 2005), so its hfs can also be neglected for our purposes.

3.5. Molybdenum

Four lines of Mo II, all connected the ground $4d^5 5s^2$ level, are of interest in this study. Three of the four upper levels of interest belong to the $4d^4(^5D)5p \text{ } z^6P^o$ term. The fourth and highest upper level is now assigned as the $4d^4(^5D)5p \text{ } z^4D^o_{5/2}$ level, but it is significantly mixed with the $4d^4(^5D)5p \text{ } z^6P^o_{5/2}$ level (Nilsson & Pickering 2003). Publications prior to the 2003 reanalysis of Mo II by Nilsson & Pickering have different assignments for the highest and lowest levels of Table 6 and have less accurate level energies than achieved in 2003 using a Fourier transform spectrometer. In addition to the transitions to the

ground level, these four upper levels have strong branches to metastable levels in the $4d^4(^5D)5s \text{ } a^6D$ term. Experimental branching fractions reported by Sikström et al. (2001) are preferred and are in a satisfactory agreement with theoretical values reported in the same paper for three of the four lines of interest. Radiative lifetimes of the four upper levels are all in the few nanosecond range due to the UV wavelengths of the highly allowed emission lines. The earlier LIF measurements of the radiative lifetimes of interest by Hannaford & Lowe (1983) do not agree with the LIF measurements by Sikström et al. Differences range from 18% to 38%, which is unusual for two sets of LIF measurements. Theoretical lifetimes reported by Sikström et al. and by Lundberg et al. (2010) are in agreement with the experimental lifetimes of Sikström et al. The primary cause of the discordant results between the two LIF experiments is very likely limitations of the fluorescence detection system used by Hannaford & Lowe. Accurate LIF measurements on lifetimes ranging down to $\sim 2 \text{ ns}$ are possible using analogue time-resolved fluorescence detection methods, but some precautions are necessary. It is essential to establish that the electronic bandwidth, linearity, and overall fidelity of the electronic detection system including the photomultiplier, cables, and digitizer (or similar recording system) are adequate for 2 ns lifetime measurements. This is best accomplished by measuring a very short benchmark life-

TABLE 6
TRANSITION PROBABILITIES FOR MO II LINES OF INTEREST

Air wavelength (Å)	E _{upper} (cm ⁻¹)	J _{upper}	E _{lower} (cm ⁻¹)	J _{lower}	A (10 ⁶ s ⁻¹)	log(<i>gf</i>)
2045.9729	48860.829	2.5	0.000	2.5	118±8	-0.35
2038.4522	49041.073	1.5	0.000	2.5	184±18	-0.34
2020.3139	49481.300	3.5	0.000	2.5	215±20	+0.02
2015.1091	49609.086	2.5	0.000	2.5	88±6	-0.49

time such as that of the resonance level of Be II, which is very well known from ab-initio theory (Weiss 1995). Tests of the combined electronic detection system are much better than tests on individual parts at GHz electronic frequencies. The selected transition probabilities of Table 6 are the experimental values of Sikström et al. Table 6 has up-to-date level energies and air wavelengths (Peck & Reeder 1972; Nilsson & Pickering 2003).

3.6. Cadmium

Only the Cd II resonance doublet from the ground $4d^{10} 5s^2 S_{1/2}$ level to the $4d^{10} 5p^2 P^o$ term is useful for stellar abundance studies. Other lines are at wavelengths that are too short or have E.P.'s that are too high, except possibly in very hot stars. The branching fractions of these UV resonance lines are 1.0 and the radiative lifetimes are known to exquisite accuracy and precision ($\sim 0.4\%$) from LIF measurements by Moehring et al. (2006) and from earlier, but somewhat less accurate, measurements by others. (See references in Moehring et al. 2006.)

There are six even isotopes with no nuclear spin and two odd isotopes with $I = 1/2$ and significant ($> 12\%$) relative abundances in natural cadmium (Böhlke et al. 2005). The unpaired s-electron in the ground level of this ion yields wide hyperfine structure (hfs) in the odd isotopes and significant isotopic structure from field shifts (nuclear volume effect). The hfs A value for the ground level of $^{113}\text{Cd}^+$ is known to exquisite accuracy and precision from radio frequency measurements by Jelenković et al. (2006). The selected hfs A values of the excited levels of $^{113}\text{Cd}^+$ are from calculations of Dixit et al. (2008b). There are older measurements of the excited level hfs A values by Brimicombe et al. (1976) that agree with the theoretical values from Dixit et al. within 0.001 cm^{-1} . We use theoretical hfs A values of Dixit et al. in part because their calculated ground level hfs A value was in much better agreement with very accurate and precise radio frequency measurements than was the experimental result from Brimicombe et al.

The ratio of the hfs A values for $^{111}\text{Cd}^+$ to that of $^{113}\text{Cd}^+$ is from Spence & McDermott (1972). Isotope shifts are from Brimicombe et al. (1976). Energy levels are from Burns & Adams (1956), and the index of air is from Peck & Reeder (1972). Tables 7 and 8 summarize the selected lab data for the Cd II resonance lines. S.S. isotopic abundances are used in Table 8 (Böhlke et al. 2005).

3.7. Ytterbium

The two UV Yb II lines of interest in this study connect the ground $4f^{14}6s^2 S_{1/2}$ level to a $J = 3/2$ level at 47005.46 cm^{-1} and a $J = 1/2$ level at 47228.96 cm^{-1} ,

both with $4f^{13}(^2F_{5/2}^o)5d6s(^1D)$ assignments. These high lying levels are not pure, but both UV lines are strongly dominant (> 0.9) branches. There is a LIF measurement of the radiative lifetime of the 47005 cm^{-1} level (Pinnington et al. 1994). The measured branching fraction for the decay of the 47005 cm^{-1} level at 2126 Å to the ground level is 0.988 (Kedzierski et al. 2010). The transition probability for the 2126 Å line from the modern LIF lifetime measurement and recent branching fraction measurement agrees beautifully with an earlier quantum calculation (Biémont et al. 1998). Without a modern experimental value for the transition probability of the 2116 Å line, it is best to use the theoretical transition probability from Biémont et al. Energy levels are from Martin et al. (1978), and wavelengths are computed using the index of air (Peck & Reeder 1972). Table 9 summarizes these data.

There are 5 stable even isotopes of ytterbium with no nuclear spin and 2 odd isotopes, ^{171}Yb with $I = 1/2$ and ^{173}Yb with $I = 5/2$, both with significant ($> 14\%$) relative abundance in natural ytterbium (Böhlke et al. 2005). The ground level has large hfs due to the unpaired s-electron, and fortunately hfs A values for the odd isotopes are well known (Münch et al. 1987; Casdorf et al. 1991). Unfortunately no hfs data are available on the excited levels at 47005 cm^{-1} and 47228 cm^{-1} . Ahmad et al. (1997) reported experimental level isotope shifts for $^{172}\text{Yb}^+$ and $^{176}\text{Yb}^+$ that can be used to determine the 2126 Å and 2116 Å isotope shift of at least these two isotopes. We have extended their measurements to other isotopes using a modified King plot as suggested by Theodossiou et al. (1997). A rough estimate is used for the ^{168}Yb isotope that has a minor (0.13%) relative abundance. Table 10 presents hfs and S.S. isotopic line component patterns for the lines of interest, but the reader is advised that the hfs A of upper levels of the odd isotopes have been neglected.

3.8. Platinum

Two of three UV Pt I lines of interest in this study connect the ground $4d^9 6s^3 D_3$ level to the $5d^8 6s 6p(^4F) ^3F_4^o$ level at 48351.94 cm^{-1} and the $5d^8 6s 6p(^4F) ^3D_3^o$ level at $48779.337 \text{ cm}^{-1}$. The third line connects the low metastable $5d^8 6s^2 ^3F_4$ level at 823.678 cm^{-1} to the $5d^8 6s 6p(^4F) ^3F_4^o$ level. The radiative lifetimes of both upper levels were measured using LIF (Den Hartog et al. 2005). Branching fractions and absolute transition probabilities were also measured for the lines at 2103 Å and 2067 Å connected to the $5d^8 6s 6p(^4F) ^3F_4$ level by Den Hartog et al. A branching fraction measurement for the third line at 2049 Å was reported by Lotrian & Guern

TABLE 7
TRANSITION PROBABILITIES FOR Cd II LINES OF INTEREST

Air wavelength (Å)	E _{upper} (cm ⁻¹)	J _{upper}	E _{lower} (cm ⁻¹)	J _{lower}	A (10 ⁶ s ⁻¹)	log(<i>gf</i>)
2265.0145	44136.173	0.5	0.00	0.5	317.7±1.1	-0.311
2144.3943	46618.532	1.5	0.00	0.5	377.8±1.4	+0.018

TABLE 8
HYPERFINE STRUCTURE AND ISOTOPIC LINE COMPONENT PATTERNS FOR Cd II LINES

Wavenumber (cm ⁻¹)	λ _{air} (Å)	F _{upper}	F _{lower}	Component Position (cm ⁻¹)	Component Position (Å)	Strength	Isotope
44136.173	2265.0145	0.5	0.5	0.07759	-0.003982	0.01250	106
44136.173	2265.0145	0.5	0.5	0.05164	-0.002650	0.00890	108
44136.173	2265.0145	0.5	0.5	0.02684	-0.001378	0.12490	110

NOTE. — Center-of-gravity wavenumbers and air wavelengths, λ_{air}, from Burns & Adams (1956), are given with component positions relative to those values. Strengths are normalized to sum to 1. Table 8 is available in its entirety via the link to the machine-readable table above.

TABLE 9
TRANSITION PROBABILITIES FOR Yb II LINES OF INTEREST

Air wavelength (Å)	E _{upper} (cm ⁻¹)	J _{upper}	E _{lower} (cm ⁻¹)	J _{lower}	A (10 ⁶ s ⁻¹)	log(<i>gf</i>)
2126.741	47005.46	1.5	0.00	0.5	50.2±1.3	-0.87
2116.675	47228.96	0.5	0.00	0.5	34.1	-1.34

TABLE 10
HYPERFINE STRUCTURE AND ISOTOPIC LINE COMPONENT PATTERNS FOR Yb II LINES

Wavenumber (cm ⁻¹)	λ _{air} (Å)	F _{upper}	F _{lower}	Component Position (cm ⁻¹)	Component Position (Å)	Strength	Isotope
47005.46	2126.741	1.5	0.5	-0.07332	0.003318	0.00130	168
47005.46	2126.741	1.5	0.5	-0.04850	0.002195	0.03040	170
47005.46	2126.741	1.5	0.5	-0.01332	0.000603	0.21830	172

NOTE. — Center-of-gravity wavenumbers and air wavelengths, λ_{air}, are from Martin et al. (1978), and the index of air (Peck & Reeder 1972) with component positions relative to those values. Strengths are normalized to sum to 1. Table 10 is available in its entirety via the link to the machine-readable table above. The hfs A values of the upper levels are neglected for the odd isotopes.

(1982). We used this measurement and the lifetime measured by Den Hartog et al. to determine its transition probability, as given in Table 11. Energy levels in Table 11 are from Blaise et al. (1992), and air wavelengths are computed from the levels using the index of air (Peck & Reeder 1972).

3.9. Mercury

Only the resonance line of Hg II at 1942 Å is potentially useful for abundance determinations in most F, G, and K stars. This line connects to the ground 5d¹⁰6s ²S_{1/2} level to the 5d¹⁰6p ²P_{1/2}^o level with a branching fraction of 1.0. The best available radiative lifetime measurement of 2.91 ± 0.11 ns is by Pinnington et al. (1988) using the Beam Foil technique with an Arbitrarily Normalized Decay Curve (ANDC) analysis. Although early Beam Foil measurements were often inaccurate due to the non-selective excitation of the method and resul-

tant cascade repopulation, this problem is eliminated using an ANDC analysis. The experimental log(*gf*) from Pinnington et al. is -0.410. A series of sophisticated quantum calculations have also been published during the last decade or so using a variety of methods. Although a single valence s-electron or p-electron outside of a closed d-shell might appear to be straightforward from a theoretical perspective, one must keep in mind that core polarization can be important, and relativistic effects are significant in an atom or ion as heavy as Hg. Brage et al. (1999) used a fully relativistic multiconfiguration Dirac-Fock method and found log(*gf*) = -0.418. Safronova & Johnson (2004) used relativistic many-body perturbation theory and found log(*gf*) = -0.369. Głowacki & Migdalek (2009) used a configuration-interaction method with numerical Dirac-Fock wave functions and found log(*gf*) = -0.381. Most recently, Simmons et al. (2011) used a variety of multi-

TABLE 11
TRANSITION PROBABILITIES FOR PT I LINES OF INTEREST

Air wavelength (Å)	E_{upper} (cm^{-1})	J_{upper}	E_{lower} (cm^{-1})	J_{lower}	A (10^6 s^{-1})	$\log(gf)$
2103.3441	48351.940	4	823.678	4	119±6	−0.15
2067.5090	48351.940	4	0.000	3	42.0±2.7	−0.62
2049.3914	48779.337	3	0.000	3	235±29	+0.02

TABLE 12
HYPERFINE STRUCTURE AND S.S. ISOTOPIC LINE COMPONENT PATTERN OF THE Hg II 1942 Å LINE

Wavenumber (cm^{-1})	λ_{vacuum} (Å)	F_{upper}	F_{lower}	Component Position (cm^{-1})	Component Position (Å)	Strength	Isotope
51486.070	1942.2729	0.5	0.5	0.44405	−0.016751	0.00150	196
51486.070	1942.2729	0.5	0.5	0.24705	−0.009320	0.09970	198
51486.070	1942.2729	0.5	0.5	0.05005	−0.001888	0.23100	200

NOTE. — Center-of-gravity wavenumbers and vacuum wavelengths, λ_{vacuum} , are for a S.S. isotopic mix from Sansonetti & Reader (2001) with component positions relative to those values. Strengths are normalized to sum to 1. Table 12 is available in its entirety via the link to the machine-readable table above.

order Coulomb as well as Coulomb-Breit approximations and found $\log(gf) = -0.363$. Based on the above experimental and theoretical results we recommend $\log(gf) = -0.40 \pm 0.04$, along with a transition wavenumber of $51486.070 \text{ cm}^{-1}$ and vacuum wavelength of 1942.2729 Å for the S.S. isotopic mix from Sansonetti & Reader (2001). We note that our recommended $\log(gf)$ does not agree with the value from Sansonetti & Reader that is currently in the Atomic Spectra Database.⁷

The wide hfs and S.S. isotopic structure of the 1942 Å line was measured quite well by Guern et al. (1977). An incredibly accurate and precise (uncertainty $< 0.001 \text{ Hz}$) radio frequency measurement of the $^{199}\text{Hg}^+$ ground level hfs splittings was published by Berkeland et al. (1998), motivated by atomic clock research. Burt et al. (2009) reported a similar measurement for $^{201}\text{Hg}^+$ ground level hfs splitting. These improved hfs A values are used to update values from Guern et al. in Table 12, but the updates shift most hfs components by $< 0.001 \text{ cm}^{-1}$. We estimate the isotope shift for ^{196}Hg , which has a low abundance of 0.15% in S.S. material. For purposes of stellar abundance analysis, the line component pattern presented in Table 12 is equivalent to that presented by Leckrone et al. (1991).

4. ABUNDANCE ANALYSIS

4.1. Model Atmospheres

HD 160617 lies relatively near the Galactic midplane ($b = -5^\circ$). Its parallax, measured by the Hipparcos mission (using the reduction validated by van Leeuwen 2007), places it at a distance of $110 \pm 20 \text{ pc}$, which is within the reddening layer. The reddening at infinity along the line of sight to HD 160617 predicted by all-sky dust maps (e.g., Schlegel et al. 1998), $E(B - V) = 0.53$, almost certainly overestimates the reddening between HD 160617 and the Sun. This interpretation finds support in the low reddening value derived from Strömgren

photometry, $E(b - y) = 0.011$ (Nissen et al. 2002), as kindly pointed out by the referee. It is inadvisable in this case to derive model atmosphere parameters by photometric methods (e.g., color-temperature relations). Instead, we derive these parameters from the spectrum of HD 160617 and comparison with a much larger sample of 153 metal-poor field subgiants from an unpublished study (I.U. Roederer et al., in preparation). This sample does not include HD 160617. We interpolate model atmospheres from the grid of Castelli & Kurucz (2003). We perform the abundance calculations using the latest version of MOOG (Sneden 1973), which includes the contribution of Rayleigh scattering from atomic H I in the source function (Sobeck et al. 2011). For this warm atmosphere, we find no difference ($< 0.01 \text{ dex}$) in the abundances derived using earlier versions of MOOG, even for lines with wavelengths short of 2000 Å .

For the large, unpublished sample, we adopt an approach using broadband colors (usually $V - K$) and 12 Gyr isochrones to make an initial estimate of the effective temperature, T_{eff} , and (logarithm of the) surface gravity, $\log g$. These values are then refined iteratively until there is no trend of Fe I abundance versus lower E.P. (used to derive T_{eff}) or line strength (used to derive the microturbulent velocity, v_t). For stars near 6000 K, that study finds a mean difference in the iron abundance derived from Fe II and Fe I of about $+0.15 \text{ dex}$ with a standard deviation of about 0.10 dex . This matches the approximate offset expected for stars at similar stellar parameters ($T_{\text{eff}} \approx 6000 \text{ K}$) and metallicities ($[\text{Fe}/\text{H}] \approx -1.8$) if departures from local thermodynamic equilibrium (LTE) are responsible (e.g., Thévenin & Idiart 1999; Mashonkina et al. 2011).

In the present study, we set T_{eff} by requiring no trend of derived Fe I abundance with E.P., and we set v_t by requiring no trend with line strength. Based on the large sample of metal-poor subgiants, we set $\log g$ by requiring $\log \epsilon (\text{Fe II}) = \log \epsilon (\text{Fe I}) + 0.15$. We set the overall metallicity of the model atmosphere equal to the iron abundance derived from Fe II. We iteratively remove

⁷ <http://www.nist.gov/pml/data/asd.cfm>

lines from the input list if their calculated abundance deviates from the mean by more than 2σ .

For HD 160617, we derive $T_{\text{eff}} = 5950$ K, $\log g = 3.90$, $v_t = 1.3$ km s $^{-1}$, and $[M/H] = -1.78$. For the subgiants in the large sample, we find typical internal (i.e., statistical) uncertainties to be $\sigma_T = 46$ K, $\sigma_{\log g} = 0.18$, $\sigma_{v_t} = 0.06$ km s $^{-1}$, and $\sigma_{[M/H]} = 0.09$. The absolute uncertainties are much more difficult to assess. Through comparisons with previous studies of the same stars in that sample (40 stars), we estimate the absolute uncertainties may be as large as $\sigma_T = 200$ K, $\sigma_{\log g} = 0.35$, $\sigma_{v_t} = 0.35$ km s $^{-1}$, and $\sigma_{[M/H]} = 0.2$. We adopt these representative uncertainties for HD 160617. Our adopted model parameters are in good (1σ internal) agreement with the means of recent studies of HD 160617: $\langle T_{\text{eff}} \rangle = 5965$ K ($\sigma = 49$ K), $\langle \log g \rangle = 3.75$ ($\sigma = 0.09$), $\langle v_t \rangle = 1.44$ km s $^{-1}$ ($\sigma = 0.12$ km s $^{-1}$), $\langle [Fe/H] \rangle = -1.74$ ($\sigma = 0.12$) (Th  venin & Idiart 1999; Gratton et al. 2000; Nissen et al. 2002, 2007; Akerman et al. 2004; Caffau et al. 2005; Jonsell et al. 2005; Asplund et al. 2006; Johnson et al. 2007; Tan et al. 2009; Hansen & Primas 2011; Peterson 2011).

4.2. Derivation of Abundances

We perform a standard EW abundance analysis for unblended lines with negligible hfs. The EWs for these lines are listed in Table 13. For all other lines we derive abundances by comparing the observed line profiles with synthetic spectra computed using MOOG. In all cases except copper we adopt the predicted r -process isotopic distribution as given in Sneden et al. (2008). For copper we adopt the S.S. isotopic distribution (B  hlke et al. 2005).

Abundances for all 377 lines examined are presented in Table 14. Abundances that are less secure are indicated by a “:” and given half weight in the final averaging. We assume a minimal internal uncertainty of 0.10 dex per line. Final mean abundances for HD 160617 are presented in Table 15.

4.3. Are We Detecting the Majority Species of These Elements?

In an LTE abundance analysis, we assume that the distribution of atoms among different level populations and ionization states can be determined by knowing the temperature and pressure (or density) at a particular layer in the atmosphere. These abundances may be in error if Boltzmann or Saha equilibrium is not satisfied. Ionization corrections for minority species account for a proportionally larger fraction of the line opacity, so abundances derived from minority species of a given element may be particularly sensitive to departures from LTE.

Several of the elements considered in the present study are rarely examined in late-type stellar atmospheres, so it is worthwhile to assess the distribution of their atoms across different ionization states. In Figure 1 we illustrate these distributions for 15 elements of interest. The temperatures shown cover the range where typical weak lines on the linear part of the curve-of-growth are formed in the atmosphere of HD 160617. Each element is found in at most three ionization stages. Figure 1 shows that first ions are the majority for most of these elements over the relevant temperature range. Substantial amounts of

neutral copper, zinc, arsenic, selenium, cadmium, tellurium, osmium, platinum, and mercury are also found. Ionization corrections for the neutral or singly-ionized states of these atoms should be reliable.

Only a few percent of the atoms of iron, strontium, molybdenum, and lead are found in the neutral state, so abundances derived from these neutral species should be viewed with more caution. Overionization of Fe I is a well-known phenomenon. The abundances of molybdenum derived from Mo I and Mo II are in good agreement in HD 160617, albeit from only one line of Mo I, but this agreement is encouraging. Mashonkina et al. (2012) have performed non-LTE line formation calculations for Pb I lines, finding positive corrections of a factor of 2 or more. This underscores the importance of deriving abundances from the majority species, although Pb II lines have not been detected in late-type stellar atmospheres.

The elements shown in Figure 1 are also representative of other heavy elements with similar ionization potentials and electronic level structures. For example, europium and lanthanum have similar first and second ionization potentials. They also have many low-lying levels that contribute similarly to the partition functions, so they should respond similarly to conditions in the stellar atmosphere. Other pairs of elements include palladium and tellurium, barium and strontium, and iridium and platinum.

In general, we are deriving abundances from the species in the majority ionization state or from minority species with a substantial presence. This certainly does not demonstrate that an LTE analysis is appropriate (e.g., Mashonkina & Gehren 2001), and we have not addressed the issue of departures from excitation equilibrium. Nevertheless, this offers some assurance that uncertainties in the ionization equilibrium are at least minimal.

5. RESULTS

5.1. UV Absorption Lines

Regions of the STIS spectrum and synthetic spectra fits around the UV lines of interest are shown in Figures 2–10. Many of these features are rarely used for stellar abundance analysis.

Four of the six Cu II lines detected in the STIS spectrum of HD 160617 are relatively unblended, as shown in Figures 2 and 3. The linelists of Kurucz & Bell (1995) suggest that the Cu II 1979.956 Å line might be blended with an Fe II line at 1979.963 Å. No experimental $\log(gf)$ value is available for this line. The Kurucz & Bell lists also indicate that the Cu II 2112.100 Å line might be blended with a weak Ni II line at 2112.107 Å. No experimental $\log(gf)$ value is available for this line, either. In both cases, we vary the strength of the blending feature within the limits allowed by the observed line profile. This introduces considerable uncertainty (0.2–0.3 dex) into the derived Cu II abundance, so we weight these lines less in the mean copper abundance. The Cu II 2135.98 Å line is clearly detected in HD 160617, but it is strong and blended with another strong Fe I line at 2135.96 Å. We do not use this line in our analysis. The mean abundance derived from the two Cu I resonance lines at 3247 Å and 3273 Å, $[Cu/Fe] = -0.87 \pm 0.07$ (internal), is about a factor of 2 lower than the mean abundance derived from the six Cu II UV lines, $[Cu/Fe] = -0.58 \pm 0.05$ (inter-

TABLE 13
EQUIVALENT WIDTH MEASUREMENTS

Wavelength (Å)	Species	E.P. (eV)	$\log(gf)$	EW (mÅ)	Instrument
5682.63	Na I	2.100	-0.706	5.3	HARPS
5688.20	Na I	2.100	-0.452	14.3	HARPS
4167.27	Mg I	4.346	-0.710	58.1	HARPS

NOTE. — Table 13 is available in its entirety in the online version of the journal. A portion is shown here to illustrate its form and content.

^a EW measured but line rejected from abundance computation; see Section 4.

TABLE 14
WAVELENGTHS, EXCITATION POTENTIALS, $\log(gf)$ VALUES, AND DERIVED ABUNDANCES

Species	Wavelength (Å) ^a	E.P. (eV)	$\log(gf)$	$\log \epsilon$	Instrument	Ref.
Be II	3130.42	0.00	-0.18	-0.35	UVES	1
Be II	3131.07	0.00	-0.48	-0.38	UVES	1
C (CH)	4290–4325	6.51	HARPS	2

REFERENCES. — (1) Fuhr & Wiese 2009; (2) B. Plez, 2007, private communication; (3) Kurucz & Bell 1995; (4) Chang & Tang 1990; (5) Aldenius et al. 2009; (6) Lawler & Dakin 1989, using hfs from Kurucz & Bell 1995; (7) Blackwell et al. 1982a,b, increased by 0.056 dex according to Grevesse et al. 1989; (8) Pickering et al. 2001, with corrections given in Pickering et al. 2002; (9) Doerr et al. 1985, using hfs from Kurucz & Bell 1995; (10) Biémont et al. 1989; (11) Sobeck et al. 2007; (12) Nilsson et al. 2006; (13) Den Hartog et al. 2011 for both $\log(gf)$ value and hfs; (14) O’Brian et al. 1991; (15) Meléndez & Barbuy 2009; (16) Cardon et al. 1982, using hfs from Kurucz & Bell 1995; (17) Nitz et al. 1999, using hfs from Kurucz & Bell 1995; (18) Blackwell et al. 1989; (19) Bielski 1975, using hfs/IS from J.S. Sobeck et al. in prep.; (20) this study; (21) Kerkhoff et al. 1980; (22) Bergeson & Lawler 1993; (23) Morton 2000; (24) Holmgren 1975, using hfs from this study; (25) Parkinson et al. 1976; (26) Biémont et al. 2011; (27) Malcheva et al. 2006; (28) Ljung et al. 2006; (29) Whaling & Brault 1988; (30) Sikström et al. 2001; (31) Wickliffe et al. 1994; (32) Xu et al. 2006; (33) Fuhr & Wiese 2009, using hfs/IS from Hansen et al. 2012; (34) Roederer et al. 2012a; (35) Fuhr & Wiese 2009, using hfs/IS from McWilliam 1998 when available; (36) Lawler et al. 2001a, using hfs from Ivans et al. 2006 when available; (37) Lawler et al. 2009; (38) Den Hartog et al. 2003, using hfs/IS from Roederer et al. 2008 when available; (39) Lawler et al. 2006, using hfs/IS from Roederer et al. 2008 when available; (40) Lawler et al. 2001b, using hfs/IS from Ivans et al. 2006; (41) Den Hartog et al. 2006; (42) Wickliffe et al. 2000; (43) Lawler et al. 2008; (44) $\log(gf)$ value from the Database on Rare Earths At Mons University (DREAM), using hfs/IS from this study; (45) Kedzierski et al. 2010, using hfs/IS from this study; (46) Sneden et al. 2009 for both $\log(gf)$ and hfs/IS; (47) Ivarsson et al. 2004; (48) Den Hartog et al. 2005; (49) Biémont et al. 2000, using hfs/IS from Roederer et al. 2012b

NOTE. — Table 14 will be available in its entirety in the final edition of the journal. Please contact the first author for an advance copy.

^a Air wavelengths are given for $\lambda > 2000$ Å and vacuum values below

nal). Cu II is by far the dominant ionization state in the atmosphere of HD 160617, and this offset may indicate the presence of significant non-LTE effects affecting Cu I.

The Zn II 2062 Å line is strong and clearly detected in our spectrum of HD 160617, as shown in Figure 4. (The 2025.48 Å Zn II line is too blended with a strong Mg I line at 2025.82 Å to be useful as an abundance indicator.) The wings of the 2062 Å line offer the most abundance sensitivity, and we ignore the line core in the fit. Calculations of the van der Waals damping parameters for this transition are not available, so we resort to the standard Unsöld (1955) approximation. The zinc abundance derived from this Zn II line is in excellent agreement with that derived from 6 Zn I lines in the optical spectral region.

We detect 3 As I lines in HD 160617, as shown in Figure 5. All are relatively unblended in HD 160617. These lines give somewhat discrepant abundance results

($\sigma = 0.37$ dex). The experimental transition probability uncertainties are comparable, and the theoretical values are in good agreement, so it is not obvious that one of these lines should be preferred over the others. We calculate the arsenic abundance in HD 160617 by taking an unweighted mean of these three lines. The fourth As I line listed in Table 3, 1937 Å, is close to the Al I auto-ionization line at 1936.46 Å. This Al I line increases the continuous opacity locally and is not well modeled by our approach, so we do not use the As I 1937 Å line as an abundance indicator.

We detect 3 Se I lines in HD 160617, as shown in Figure 6. The 1960 Å line is clearly saturated and not on the linear part of the curve of growth. The 2039 Å line is blended with a Cr I line at 2039.92 Å, which can be fit by our synthesis. The 1960 Å and 2074 Å lines are unblended in HD 160617. All 3 lines give similar abundance results ($\sigma = 0.08$).

TABLE 15
MEAN ABUNDANCES IN HD 160617

Z	Species	$\log \epsilon$ S.S. ^a	$\log \epsilon$	[X/Fe] ^b	N_{lines}	σ_{internal}	σ_{total}
4	Be II	1.38	-0.36	+0.03	2	0.07	0.30
6	C (CH)	8.43	+6.61	+0.10	...	0.15	0.25
7	N (NH)	7.83	+6.51	+0.60	...	0.15	0.25
8	O (OH)	8.69	+7.22	+0.45	...	0.15	0.25
11	Na I	6.24	+4.58	+0.26	2	0.07	0.20
12	Mg I	7.60	+5.88	+0.20	4	0.23	0.30
14	Si I	7.51	+5.91	+0.32	3	0.07	0.20
20	Ca I	6.34	+4.78	+0.36	13	0.09	0.21
21	Sc II	3.15	+1.45	+0.07	8	0.15	0.33
22	Ti I	4.95	+3.31	+0.28	16	0.04	0.19
22	Ti II	4.95	+3.47	+0.29	28	0.08	0.30
23	V I	3.93	+2.08	+0.07	1	0.10	0.33
23	V II	3.93	+2.34	+0.18	2	0.07	0.30
24	Cr I	5.64	+3.62	-0.10	13	0.05	0.20
24	Cr II	5.64	+4.08	+0.21	3	0.06	0.30
25	Mn I	5.43	+3.19	-0.32	5	0.04	0.19
25	Mn II	5.43	+3.37	-0.29	6	0.04	0.29
26	Fe I	7.50	+5.58	-1.92 ^c	119	0.06	0.20
26	Fe II	7.50	+5.73	-1.77 ^d	11	0.05	0.29
27	Co I	4.99	+3.07	+0.00	7	0.13	0.23
28	Ni I	6.22	+4.30	+0.00	14	0.05	0.20
29	Cu I	4.19	+1.40	-0.87	2	0.07	0.20
29	Cu II	4.19	+1.84	-0.58	6	0.05	0.29
30	Zn I	4.56	+2.76	+0.12	6	0.05	0.20
30	Zn II	4.56	+2.94	+0.15	1	0.10	0.31
32	Ge I	3.65	< +1.20	< -0.53
33	As I	2.30	+0.60	+0.22	3	0.37	0.42
34	Se I	3.34	+1.56	+0.14	3	0.08	0.21
38	Sr I	2.87	+0.85	-0.10	1	0.10	0.21
38	Sr II	2.87	+1.22	+0.12	3	0.09	0.30
39	Y II	2.21	+0.25	-0.19	11	0.08	0.30
40	Zr II	2.58	+1.05	+0.24	20	0.07	0.30
42	Mo I	1.88	+0.58	+0.62	1	0.10	0.22
42	Mo II	1.88	+0.61	+0.50	4	0.09	0.30
44	Ru I	1.75	+0.59	+0.76	1	0.10	0.22
46	Pd I	1.65	-0.07	+0.20	1	0.10	0.22
47	Ag I	1.20	-0.89	-0.17	1	0.20	0.28
48	Cd II	1.71	-0.03	+0.03	1	0.10	0.31
52	Te I	2.18	+0.67	+0.41	1	0.20	0.32
56	Ba II	2.18	+0.44	+0.03	2	0.07	0.30
57	La II	1.10	-0.36	+0.31	4	0.07	0.30
58	Ce II	1.58	+0.06	+0.25	9	0.09	0.30
60	Nd II	1.42	-0.03	+0.32	4	0.09	0.30
62	Sm II	0.96	-0.45	+0.36	3	0.15	0.33
63	Eu II	0.52	-0.81	+0.44	4	0.05	0.29
64	Gd II	1.07	-0.30	+0.40	3	0.06	0.30
66	Dy II	1.10	-0.20	+0.47	6	0.04	0.29
68	Er II	0.92	-0.35	+0.50	3	0.06	0.30
70	Yb II	0.92	-0.42	+0.43	3	0.15	0.33
76	Os II	1.40	-0.12	+0.25	1	0.20	0.36
77	Ir II	1.38	+0.35	+0.74	1	0.10	0.31
78	Pt I	1.62	+0.44	+0.74	3	0.10	0.21
80	Hg II	1.17	< +0.40	< +1.00
82	Pb I	2.04	< +0.90	< +0.78

^a Solar abundances from Asplund et al. (2009)

^b Abundance ratios for neutrals are computed relative to Fe I and abundance ratios for ions are computed relative to Fe II

^c [Fe I/H]

^d [Fe II/H]

We detect one unblended line of Zr II in the STIS spectrum of HD 160617, 1996 Å, as shown in Figure 4. The abundance derived from this line is in excellent agreement with the abundance derived from the 19 Zr II lines in the optical spectral range (3095 Å–4208 Å). This indicates that any possible offset between the optical and UV abundance scales (due to, e.g., inaccurate calculation of the continuous opacity) is small.

We detect 4 Mo II lines in HD 160617, as shown in Figure 7. These lines are relatively clean and provide

similar abundance results ($\sigma = 0.09$). The abundance derived from these lines agrees with the abundance derived from the Mo I line at 3864 Å, although we recall from Section 4.3 that very little neutral molybdenum is present in the line-forming layers of HD 160617. Peterson (2011) also derived a molybdenum abundance from these Mo II lines in the same STIS spectrum of HD 160617. After correcting for the different $\log(gf)$ scales used, our [Mo/Fe] ratio is about 0.4 dex lower than hers. This discrepancy is larger than can be accounted

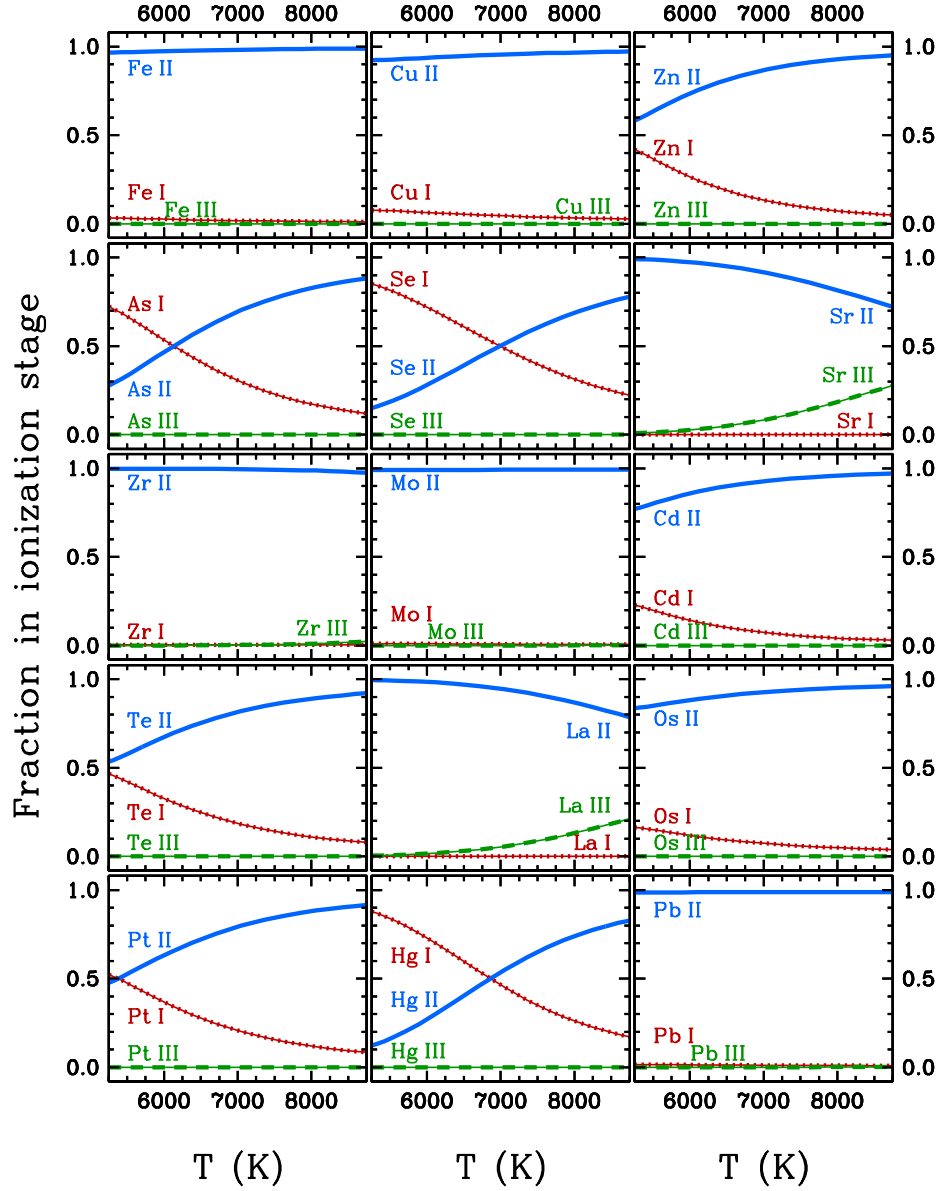


FIG. 1.— Illustration of the ionization distribution for 15 elements of interest in the atmosphere of HD 160617. The fraction of an element in the neutral state is shown by the red studded curves. The fraction in the first ionized state is shown by the blue solid curves. The fraction in the second ionized state is shown by the green dashed curves. The temperature range shown corresponds to the main line-forming layers for weak lines ($\log EW/\lambda < -4.7$) in the atmosphere of HD 160617. For weak lines with low E.P. values, $>99\%$ of the line opacity is found between 5500 K and 8500 K in this model atmosphere.

for by the slight differences in model atmosphere parameters ($\delta T_{\text{eff}} = 50$ K, $\delta \log g = 0.1$, $\delta v_t = 0.1$ km s $^{-1}$), and the line-by-line differences cannot be assessed from the published data. Regardless, the molybdenum in HD 160617 is still overabundant, a curious fact that Peterson discussed in detail. The possibility that a small amount of s -process material may be present in HD 160617 (Section 6.3) is an unlikely explanation for the molybdenum overabundance.

We detect the Cd II 2144.39 Å line in HD 160617, as shown in Figure 8. This line is blended with Fe II 2144.35 Å and Fe I 2144.44 Å. These blends can be adjusted to fit the line profile. The residual absorption can be well fit by the Cd II line.

The Te I 2142.822 Å line in HD 160617 is very blended

with Fe I 2142.832 Å. No experimental $\log(gf)$ value is known for the Fe I line. These lines are separated just enough to break the $\log(gf)$ -abundance degeneracy in the high-resolution STIS spectrum. We estimate the strength of the Fe I line by fitting the line profile with a combination of Te I and Fe I absorption. We include absorption from an extra, unidentified line at 2142.87 Å. We can produce a reasonable fit to the Te I 2142 Å line, but we caution that the uncertainty in the derived abundance surely is larger than the uncertainties of other, unblended absorption features.

We detect 2 Yb II absorption lines in the STIS spectrum, 2116 Å and 2126 Å, shown in Figure 9, as well as the more common optical Yb II line at 3694 Å. The abundance derived from the 2116 Å line is a factor of 2 greater

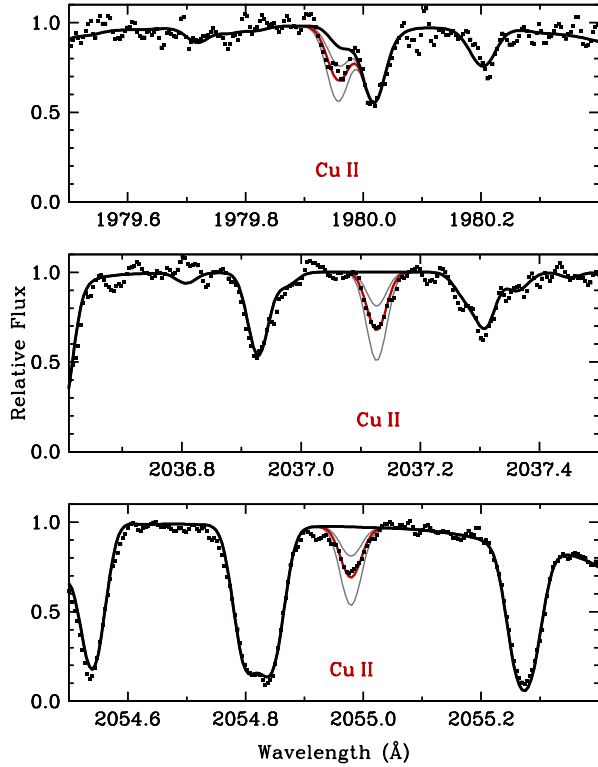


FIG. 2.— Synthesis of three Cu II lines in the UV. The observed STIS spectrum is marked by the filled squares. The best-fit synthesis is indicated by the bold red line, and the light gray lines show variations in the best-fit abundance by ± 0.3 dex. The bold black line indicates a synthesis with no Cu II present.

than that derived from the other two lines, which are in good agreement. The general agreement is reassuring for studies where only the 3694 Å line is available.

We report a marginal detection of the Os II line at 2067 Å, as shown in Figure 10. This line is weak and the spectrum is noisy here, so the abundance should be interpreted with caution. The other Os I or Os II abundance indicators commonly detected in *r*-process rich metal-poor stars are not covered by existing spectra of HD 160617.

We detect one Ir II line in HD 160617, as shown in Figure 9. This line appears to be blended with a weak, high-excitation Ni II line at 2126.83 Å. No experimental $\log(gf)$ value is available for this Ni II line. We fit the line profile as best as possible. None of the common UV Ir I abundance indicators are covered by existing spectra of HD 160617.

We detect 3 Pt I lines in HD 160617, as shown in Figure 10. Two of these lines, 2067 Å and 2049 Å, are relatively clean. The third line, 2103 Å, is detected as extra absorption between two stronger lines. Our syntheses do not predict absorption from other species between 2103.5 Å and 2103.65 Å, whereas the observed spectrum clearly indicates absorption. The abundance derived from this Pt I line is much less secure, and we weight it half as much as the other two lines in the average. Nevertheless, the abundances of all three lines are in good agreement ($\sigma = 0.10$).

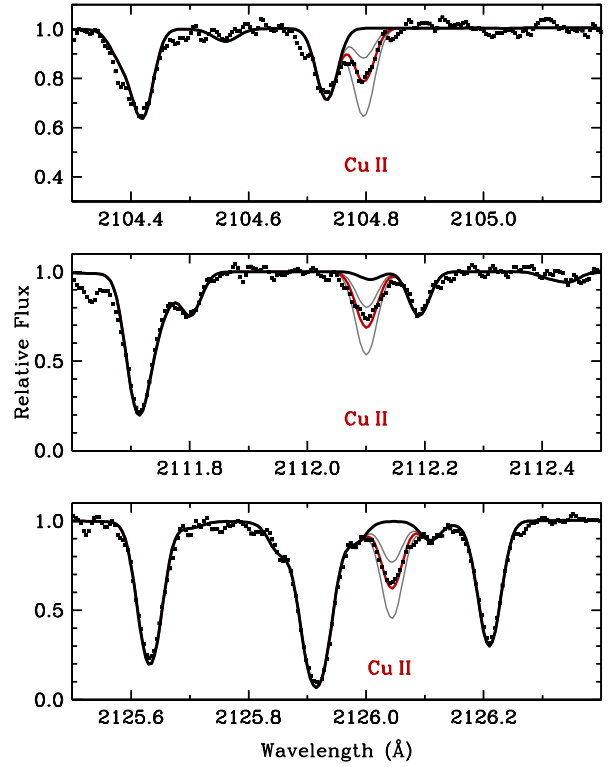


FIG. 3.— Synthesis of three Cu II lines in the UV. The observed STIS spectrum is marked by the filled squares. The best-fit synthesis is indicated by the bold red line, and the light gray lines show variations in the best-fit abundance by ± 0.3 dex. The bold black line indicates a synthesis with no Cu II present.

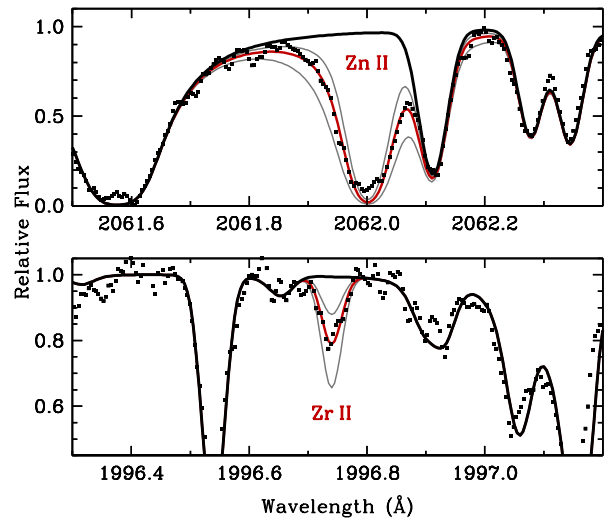


FIG. 4.— Synthesis of the Zn II and Zr II lines in the UV. The observed STIS spectrum is marked by the filled squares. The best-fit synthesis is indicated by the bold red line, and the light gray lines show variations in the best-fit abundance by ± 0.3 dex. The bold black line indicates a synthesis with no Zn II or Zr II present.

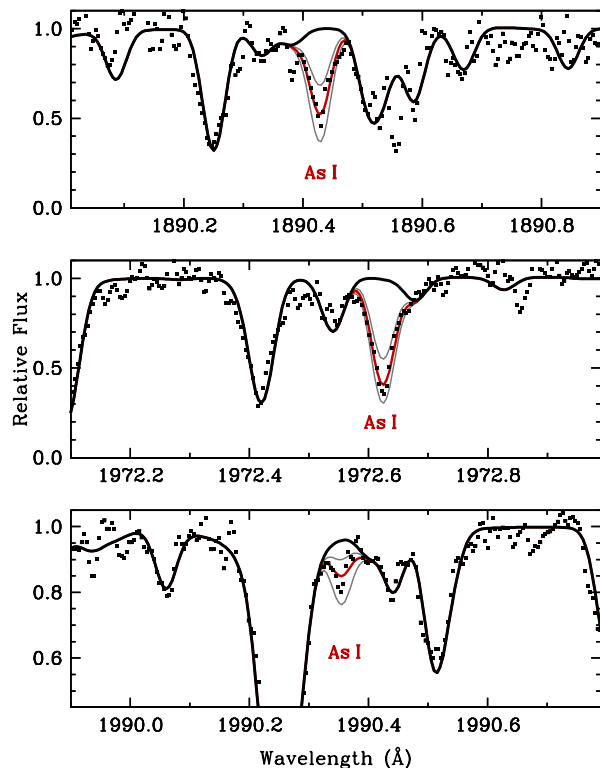


FIG. 5.— Synthesis of the As I lines in the UV. The observed STIS spectrum is marked by the filled squares. The best-fit synthesis is indicated by the bold red line, and the light gray lines show variations in the best-fit abundance by ± 0.3 dex. The bold black line indicates a synthesis with no As I present.

We do not detect the Hg II 1942.27 Å absorption line in HD 160617. We synthesize the line and derive an upper limit on the mercury abundance.

5.2. Other Abundances

We have derived abundances for all Fe-group elements from calcium to zinc. We have detected multiple ionization stages for several of these elements, including titanium, vanadium, chromium, manganese, iron, copper, and zinc. The [Ti/Fe], [V/Fe], [Mn/Fe], and [Zn/Fe] ratios derived from neutral atoms and single ions are in agreement in HD 160617. These elements are mostly ionized in the line-forming regions of HD 160617, so this agreement is gratifying. We recover the persistent disagreement between [Cr/Fe] ratios derived from neutral atoms and ions (e.g., Gratton & Sneden 1991; Sobeck et al. 2007; Bergemann & Cescutti 2010, and references therein), $[\text{Cr II}/\text{Fe II}] - [\text{Cr I}/\text{Fe I}] = +0.31$ dex. We also find a similar offset between neutral and ionized copper, $[\text{Cu II}/\text{Fe II}] - [\text{Cu I}/\text{Fe I}] = +0.29$ dex.

Hansen & Primas (2011) studied the palladium and silver abundances in a large sample of dwarf and giant metal-poor stars, including HD 160617. Our [Pd/Fe] ratio is in good agreement with theirs. They only reported an upper limit on [Ag/Fe]. We report a tentative detection of the weak Ag I line at 3382 Å. The abundance derived from this line is consistent with their reported upper limit. Most of the silver in the line-forming layers of HD 160617 is Ag II, so our abundance should be

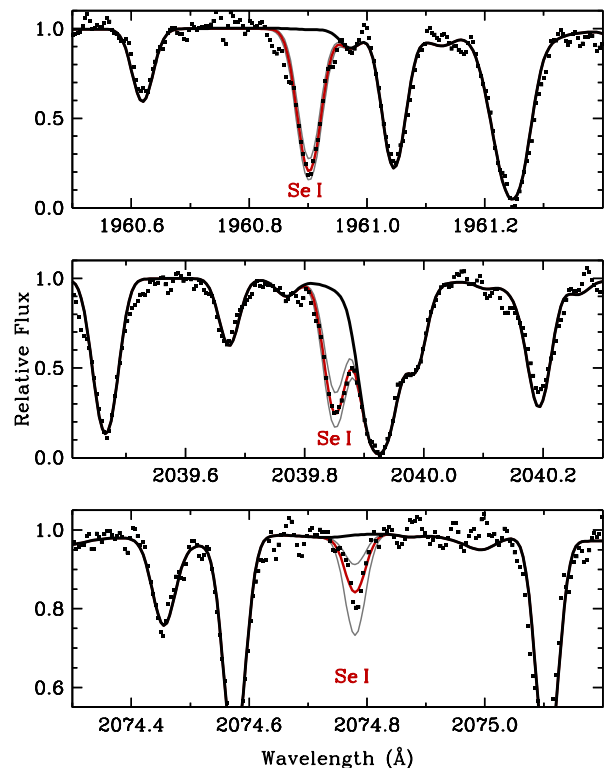


FIG. 6.— Synthesis of the Se I lines in the UV. The observed STIS spectrum is marked by the filled squares. The best-fit synthesis is indicated by the bold red line, and the light gray lines show variations in the best-fit abundance by ± 0.3 dex. The bold black line indicates a synthesis with no Se I present.

viewed with caution. The lower-lying levels of Ag I are all known, fortunately, so the partition functions of Ag I should be relatively complete. The first ionization potential of silver is 7.58 eV, nearly the same as copper, 7.73 eV, which has a similar electronic configuration. By analogy, Figure 1 suggests that no more than a few percent of the silver is present as Ag I. The strongest transitions of Ag II lie deep in the vacuum UV, and there is little hope of detecting these lines in late-type stars. The first ionization potential of palladium is somewhat higher, 8.34 eV, but not as high as cadmium, 8.99 eV, so a small amount of Pd I may be present.

6. DISCUSSION

6.1. Nucleosynthesis of Arsenic and Selenium and Their Abundances beyond the Solar System

CI chondrite meteorites reveal that selenium is the second most abundant element heavier than zinc in the S.S.; arsenic is the ninth most abundant. Isotopes of each can be produced by both s -process and r -process nucleosynthesis. In S.S. material, the s -process contribution to these elements is predicted to be small, ≈ 5 –10% (e.g., Arlandini et al. 1999; Bisterzo et al. 2011). While the flow of r -process nucleosynthesis should pass through the parent isobars of these elements, other mechanisms may also contribute to their production in environments traditionally ascribed to the r -process. These include a charged-particle (α) process (e.g., Woosley & Hoffman 1992; Farouqi et al. 2009) or a weak r -process in nu-

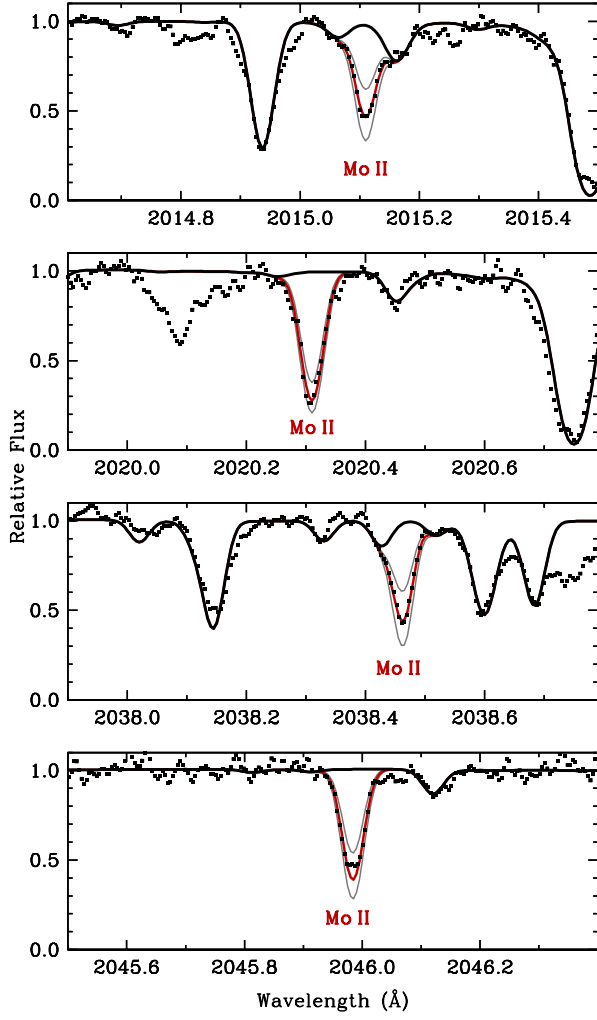


FIG. 7.— Synthesis of the Mo II lines in the UV. The observed STIS spectrum is marked by the filled squares. The best-fit synthesis is indicated by the bold red line, and the light gray lines show variations in the best-fit abundance by ± 0.3 dex. The bold black line indicates a synthesis with no Mo II present.

clear statistical equilibrium with a small neutron excess (Wanajo et al. 2011). Calculations of r -process nucleosynthesis using the “waiting-point” approximation and a weighting of neutron density components can reproduce the predicted S.S. r -process elemental abundance of selenium (e.g., Kratz et al. 2007; Farouqi et al. 2009).

The elements arsenic and selenium have not been detected previously in halo stars, and neither has been detected in the solar photosphere. As I and II lines in the UV have been detected in chemically-peculiar stars, including χ Lupi (e.g., Leckrone et al. 1999, and references therein). Cardelli et al. (1993) detected As II and Se II in the interstellar medium (ISM) towards ζ Oph. [Se IV] is detected in emission in planetary nebulae, where its abundance can frequently be attributed to self-enrichment by the s -process (Dinerstein 2001; Sterling & Dinerstein 2008). This same line has also been found in ultra-compact H II regions in the vicinity of hot O stars (Blum & McGregor 2008; Roman-Lopes et al. 2009). Chayer et al. (2005) reported

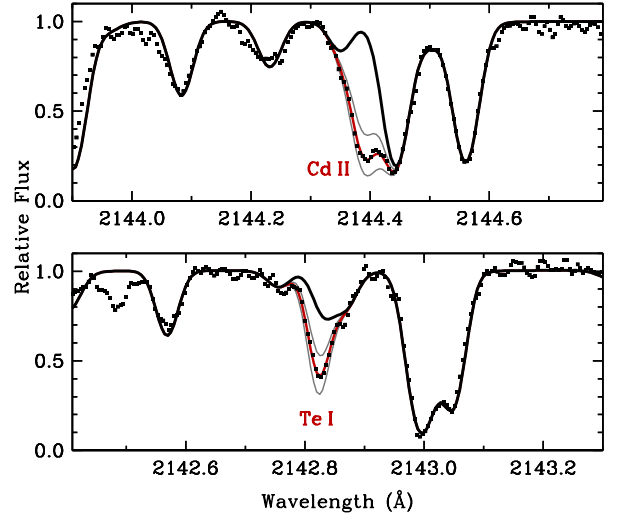


FIG. 8.— Synthesis of the Cd II and Te I lines in the UV. The observed STIS spectrum is marked by the filled squares. The best-fit synthesis is indicated by the bold red line, and the light gray lines show variations in the best-fit abundance by ± 0.3 dex. The bold black line indicates a synthesis with no Cd II or Te I present.

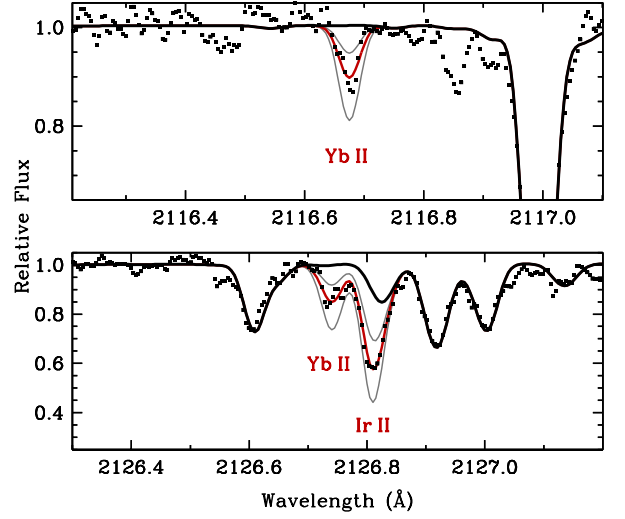


FIG. 9.— Synthesis of the Yb II and Ir II lines in the UV. The observed STIS spectrum is marked by the filled squares. The best-fit synthesis is indicated by the bold red line, and the light gray lines show variations in the best-fit abundance by ± 0.3 dex. The bold black line indicates a synthesis with no Yb II or Ir II present.

the detection of several high-ionization absorption lines of arsenic and selenium in the far UV spectrum of a hydrogen-deficient white dwarf, although Boyce et al. (2008) suggest that these are likely misidentifications of ISM lines or photospheric lines of lighter ions. None of these detections offers the same opportunity that HD 160617 does to study detailed (r -process) nucleosynthesis patterns including arsenic and selenium.

6.2. How Normal Is HD 160617?

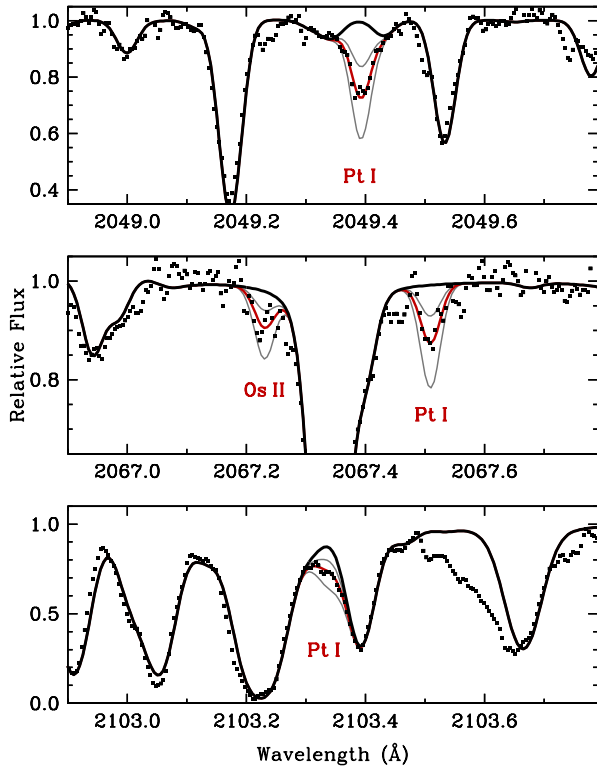


FIG. 10.— Synthesis of the Os II and Pt I lines in the UV. The observed STIS spectrum is marked by the filled squares. The best-fit synthesis is indicated by the bold red line, and the light gray lines show variations in the best-fit abundance by ± 0.3 dex. The bold black line indicates a synthesis with no Os II or Pt I present.

HD 160617 is an old (11.7 ± 2.1 Gyr) star with kinematics consistent with membership in the Galactic halo (Holmberg et al. 2007). Holmberg et al. also find that HD 160617 shows no evidence of radial velocity variations over a long (12 yr) baseline, indicating that it is not in a binary system. de Medeiros et al. (2006) find a low rotational velocity ($v \sin i = 6.2 \pm 2.6$ km s $^{-1}$) for HD 160617. These are typical characteristics for field stars at the metallicity of HD 160617, $[\text{Fe}/\text{H}] = -1.8$. Several studies of the composition of HD 160617 over the last 30 years have suggested that abundances of some of the light ($Z \leq 30$) elements in this star may be anomalous. Here, we reconsider these matters in light of the high-quality spectra of this star now available.

The α and Fe-group abundances in HD 160617 fall well within the usual trends for stars at this metallicity, as established by previous studies (Gratton & Sneden 1991; Fulbright 2002; Sobeck et al. 2006; Nissen et al. 2007; Primas & Sobeck 2008; Roederer et al. 2010b). The $[\text{O}/\text{Fe}]$, $[\text{Mg}/\text{Fe}]$, $[\text{Si}/\text{Fe}]$, $[\text{Ca}/\text{Fe}]$, and $[\text{Ti}/\text{Fe}]$ ratios are all enhanced by factors of 1.6 to 2.8, typical for metal-poor halo stars enriched by core-collapse supernovae. Nissen et al. (2007) found that the $[\text{S}/\text{Fe}]$ ratio in HD 160617 is also enhanced by a similar factor. The $[\text{Na}/\text{Fe}]$ ratio in HD 160617 lies on the upper envelope of the $[\text{Na}/\text{Fe}]$ ratios found in field stars, but there is considerable scatter in $[\text{Na}/\text{Fe}]$ at this metallicity (e.g., Pilachowski et al. 1996; Gratton et al. 2000). The abun-

dance ratios among Fe-group elements are unremarkable.

Observations by Bessell & Norris (1982) and Laird (1985) found $[\text{N}/\text{Fe}]$ to be significantly enhanced in HD 160617 by a factor of 50–100 relative to the solar ratio. Subsequent studies by Zhao & Magain (1990) and Johnson et al. (2007) have found much lower levels of nitrogen enhancement (factors of 2.5–6). Our nitrogen abundance, derived from NH, supports the lower value. Nevertheless, this $[\text{N}/\text{Fe}]$ ratio is still somewhat higher than that found in typical field stars (e.g., Gratton et al. 2000; Israelian et al. 2004). The $[\text{C}/\text{Fe}]$ ratio in HD 160617, derived by us from CH, is approximately solar. We are limited by systematic uncertainties inherent to deriving abundances from hydride bands (continuum placement or large corrections from a 1-dimensional to a 3-dimensional model atmosphere, for example) and offsets introduced by using different abundance indicators (e.g., Tomkin et al. 1992). We shall not dwell on the issue of carbon and nitrogen abundances except to say that nitrogen may be mildly enhanced in HD 160617.

Primas et al. (1998) found that the boron abundance in HD 160617 is unusually low for its evolutionary state, yet the lithium abundance in HD 160617 is consistent with that of the Spite plateau for metal-poor dwarf and subgiant stars. Those authors noted that the abundance of beryllium, the element between lithium and boron, in HD 160617 is uncertain. Examination of Figure 3 of Molaro et al. (1997) reveals that the S/N of the UVES spectrum employed in the present study is significantly higher than what was available previously. Using the UVES spectrum, we derive a beryllium abundance from the Be II 3130.42 Å and 3131.07 Å doublet. The hfs of these lines can be neglected in the abundance analysis. This abundance is in good agreement with more recent work (Tan et al. 2009) and falls well within the Galactic trends of $A(\text{Be})$ versus $[\text{Fe}/\text{H}]$ or $[\text{O}/\text{H}]$ (e.g., Boesgaard et al. 2011). This suggests that beryllium is not depleted in HD 160617 relative to other halo stars.

The unexplained low boron abundance and slight nitrogen enhancement notwithstanding, the kinematics and composition of HD 160617 suggest that it is a normal, metal-poor halo star passing through the Solar neighborhood.

6.3. The Heavy Element Abundance Pattern in HD 160617

Figure 11 shows the heavy element abundance pattern in HD 160617. In the legend, we highlight elements that can only be detected in the UV using *HST*. These elements comprise 30% of all heavy elements detected in HD 160617, including all of the elements detected at the three r -process peaks. This striking illustration demonstrates the unique opportunity made available by placing sensitive UV echelle spectrographs in space.

In Figure 11, abundances derived from neutral atoms are shown with open squares, and abundances derived from ions are shown with filled squares. To account for the difference between $[\text{Fe I}/\text{H}]$ and $[\text{Fe II}/\text{H}]$ in HD 160617, for display purposes in Figure 11 we shift the abundances derived from neutral atoms upward by 0.15 dex. The overall normalization between the neutrals and ions is somewhat uncertain, so ratios between elements detected in different ionization states should be

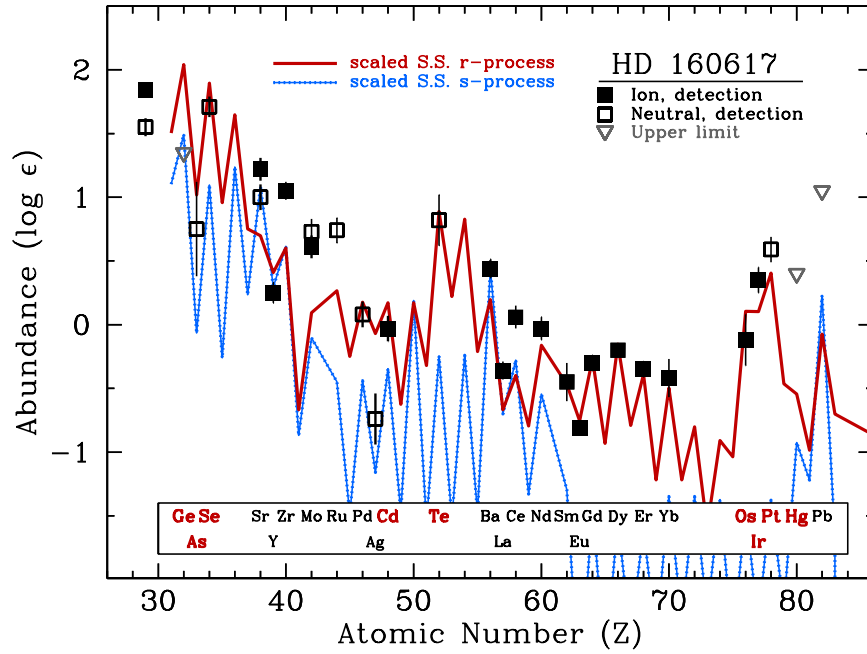


FIG. 11.— Logarithmic abundances in HD 160617 as a function of atomic number. Abundances derived from neutral species are shown as open squares, and abundances derived from singly-ionized species are shown as filled squares. Error bars represent internal uncertainties only. The abundances of neutral species have been offset vertically in this figure by +0.15 dex to reflect the difference between $[\text{Fe I}/\text{H}]$ and $[\text{Fe II}/\text{H}]$. Open, downward-facing triangles mark upper limits. The bold, solid red curve indicates the scaled S.S. r -process residuals, scaled to match the heavy rare earth element abundances (Sm–Yb) in HD 160617. The studded blue curve indicates the scaled S.S. s -process predictions, scaled to match the barium abundance in HD 160617. These predictions are taken from Sneden et al. (2008), but the lead and bismuth predictions have been taken from the low-metallicity stellar models of Bisterzo et al. (2011). Symbols of elements that can only be detected in the UV from space-based spectra are shown in bold red letters in the box at the bottom.

interpreted with caution (e.g., $[\text{Se}/\text{Zr}]$, $[\text{Pd}/\text{Cd}]$, $[\text{Cd}/\text{Te}]$, $[\text{Te}/\text{Eu}]$, and $[\text{Pt}/\text{Ir}]$). Ratios constructed among elements derived from the same ionization state should be much more secure (e.g., $[\text{As}/\text{Se}]$, $[\text{Se}/\text{Te}]$, $[\text{La}/\text{Eu}]$, and $[\text{Te}/\text{Pt}]$).

Scaled versions of the predicted S.S. s - and r -process distributions are also shown in Figure 11. There are natural limitations to the utility of these predictions, but they are useful first approximations to interpret the heavy element enrichment patterns. The r -process distribution provides a fair fit to the observed abundance pattern in HD 160617, while the s -process distribution does not. The r -process distribution matches the elements at the heavy end of the rare earth domain (samarium through ytterbium) and the third r -process peak elements (osmium through platinum). When normalized to these elements, the elements at the light end of the rare earth domain (barium through neodymium) appear slightly overabundant in HD 160617. Some of the lighter elements (strontium, zirconium, molybdenum, and ruthenium) also appear overabundant, others nearly match the predictions (arsenic, selenium, yttrium, palladium, cadmium, and tellurium), and others (germanium, silver) appear underabundant. No alternative normalization of the scaled S.S. r -process distribution can provide a satisfactory match to all the elements from germanium to tellurium.

At least one element at each r -process peak has been detected in the neutral state: selenium, tellurium, and platinum. We recall from Section 5.1 that the only line of Te I available in our spectrum of HD 160617 is quite blended, so the uncertainty here is considerably larger.

All three of these abundances are close to their predicted values in the scaled S.S. r -process residuals. If the abundances of osmium and iridium, derived from transitions among ions, are also considered, the overall agreement of the three r -process peaks must be considered quite good.

In Figure 12, we compare the abundances in HD 160617 with those in HD 108317 (Roederer et al. 2012b). The overall metallicity of HD 108317 is a factor of 4 lower than that of HD 160617, but both stars have very similar heavy element enrichment levels, $[\text{Eu}/\text{Fe}] \approx +0.4$. Despite its overall lower metallicity, we were able to detect more elements in HD 108317 because it is a red giant with a lower continuous opacity. For the 22 elements in common from strontium to platinum, the overall agreement between the two stars is striking. We previously suggested that HD 108317 may contain a small amount of s -process material in addition to a substantial r -process foundation. The predicted abundances for the elements at the three r -process peaks do not change appreciably if a small amount of s -process material is present (Roederer et al. 2012b). Another possible explanation is that both patterns are produced by r -process nucleosynthesis (or mechanisms that may occur alongside the r -process, such as charged-particle freeze-out; e.g., Woosley & Hoffman 1992; Farouqi et al. 2010). HD 160617 and HD 108317 could be considered intermediate cases between the extreme r -process abundance patterns found in the metal-poor stars CS 22892–052 (Sneden et al. 2003) and HD 122563 (Honda et al. 2006; Roederer et al. 2012b).

This overall agreement between HD 160617 and HD 108317 allows us to confront systematic effects in

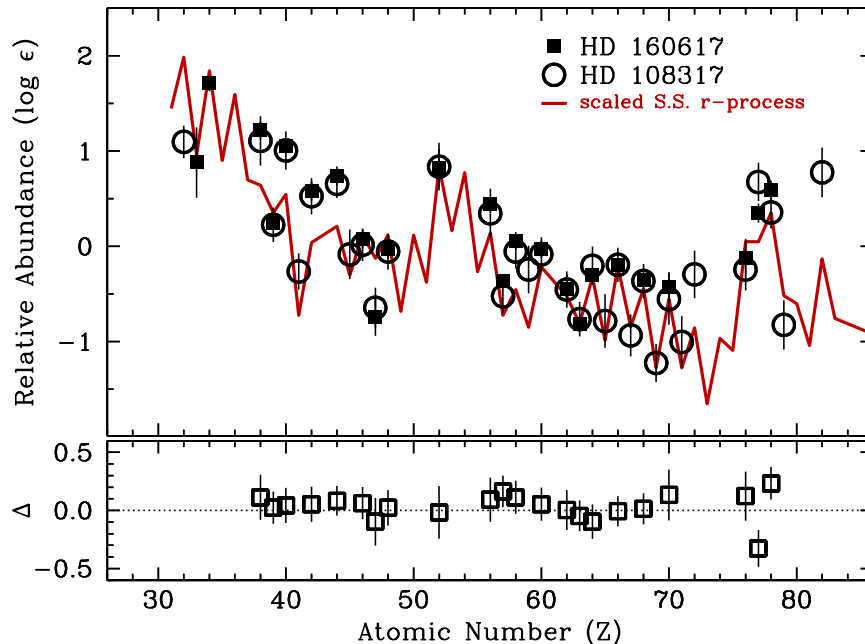


FIG. 12.— Comparison of the abundances in HD 160617 and HD 108317 (Roederer et al. 2012b). The filled squares indicate the abundances in HD 160617, the open circles indicate the abundances in HD 108317, and the solid red line marks the scaled S.S. r -process residuals, normalized to the heavy rare earth abundances (Sm–Yb) in HD 160617. The abundances of neutral species in HD 160617 and HD 108317 have been offset vertically in this figure by +0.15 dex and +0.18 dex to reflect the differences between $[\text{Fe I}/\text{H}]$ and $[\text{Fe II}/\text{H}]$. The open squares in the bottom panel show the differences between these two stars (in the sense of HD 160617 minus HD 108317). Uncertainties in the bottom panel are computed as $((\sigma_{\text{HD 160617}}^2 + \sigma_{\text{HD 108317}}^2)/2)^{1/2}$.

the abundance analysis. In HD 160617, the cadmium abundance has been derived from one line of Cd II. In HD 108317, the cadmium abundance has been derived from one line of Cd I. The fact that both lines give similar relative abundances may hint that both indicators are generally reliable. Similarly, the agreement between the relative tellurium abundances that have been derived from two different Te I lines (2142 Å and 2385 Å) lends confidence to both lines. For the third r -process peak elements osmium, iridium, and platinum, the agreement is less good. Critical comparison of the relative abundance patterns among these three elements may not yet be warranted.

Strong odd-even Z effects are observed in both HD 160617 and HD 108317. These effects are predicted by the scaled S.S. r -process residuals for the rare earth elements between the second and third r -process peaks. These effects are generally not predicted for the elements from strontium through cadmium. This phenomenon has noticed before (Sneden et al. 2000; Johnson & Bolte 2002; Farouqi et al. 2009; Roederer et al. 2010a), but the growing number of elements detected from multiple transitions of the dominant ionization stage lends considerable weight to its existence. Stronger odd-even effects are more commonly associated with s -process nucleosynthesis. The amount of s -process material required to reproduce the observed effect in HD 160617 and HD 108317 exceeds the total abundance of, e.g., strontium, zirconium, or barium in these stars. We regard an s -process origin for this odd-even effect as unlikely.

We detect a similar odd-even effect for arsenic and selenium. This is predicted by the scaled S.S. r -process residuals, though the application of the r -process residual calculation method at these low atomic numbers is

questionable. The germanium abundance in HD 108317 and our upper limit in HD 160617 suggest that the odd-even effect does not extend to this transition element. The germanium abundances in these two stars are consistent with the trends identified by Cowan et al. (2005), indicating a correlation between $[\text{Ge}/\text{H}]$ and $[\text{Fe}/\text{H}]$. Simulations of nucleosynthesis in the high-entropy wind of core-collapse supernovae predict that germanium production should be decoupled from the main r -process (e.g., Farouqi et al. 2009), as is observed. These simulations predict that arsenic and selenium should also be decoupled, which appears to contrast with our observations of HD 160617. The fact that arsenic and selenium more-or-less conform to the scaled S.S. r -process residuals, while germanium clearly deviates, could indicate that this is the point where the r -process turns on. Additional observations of these three elements in other metal-poor stars will be necessary to help resolve the matter.

7. CONCLUSIONS

We have used archive space- and ground-based spectra to study detailed abundances in the metal-poor subgiant star HD 160617. We have derived abundances of 51 species of 42 elements in HD 160617, plus upper limits for 3 more. This inventory includes 27 elements heavier than zinc that are produced at least in part by n -capture reactions. For the first time, we have detected elements at all three r -process peaks in a Galactic halo star: the first r -process peak element selenium, the second r -process peak element tellurium, and the third r -process elements osmium, iridium, and platinum. This advance is made possible by the high resolution UV spectrum of HD 160617 taken with STIS on *HST*, covering $1879 < \lambda < 2148$ Å. We review the literature and present

up-to-date transition probabilities and, when available, line component patterns including the effects of hfs and IS for Cu II, Zn I and II, As I, Se I, Mo II, Cd II, Yb II, Pt I, and Hg II.

The heavy elements in HD 160617 were produced primarily by *r*-process nucleosynthesis. When the scaled S.S. *r*-process residuals are normalized to the rare earth elements in HD 160617, the elements at the three *r*-process peaks have abundances that nearly match the scaled S.S. *r*-process residuals. This result reaffirms, on the basis of critical elements detected for the first time, many previous suggestions that the nucleosynthesis that occurred in the early universe resembles later *r*-process events that produced about half the heavy elements in the S.S. On the other hand, this result may be somewhat surprising, since the production of arsenic and selenium is predicted to be decoupled from that of the *r*-process elements at the second peak and beyond. Our non-detection of germanium in HD 160617 indicates that this element does not follow the scaled S.S. *r*-process residuals. We leave it as a challenge to theory to find a nucleosynthesis model capable of reproducing the observed abundance patterns in this star.

We thank the referee for providing an extremely rapid and helpful report, and we thank C. Hansen and J. Sobeck for sending results in advance of publication. I.U.R. thanks G. Preston for sharing his copy of Paul Merrill's monograph, "Lines of the Chemical Elements In Astronomical Spectra." This research has made use of NASA's Astrophysics Data System Bibliographic Services, the arXiv pre-print server operated by Cornell University, the SIMBAD and VizieR databases hosted by the Strasbourg Astronomical Data Center, the Atomic Spectra Database hosted by the National Institute of Standards and Technology, the Multimission Archive at the Space Telescope Science Institute, the ESO Science Archive Facility, and the Keck Observatory Archive. IRAF is distributed by the National Optical Astronomy Observatories, which are operated by the Association of Universities for Research in Astronomy, Inc., under co-operative agreement with the National Science Foundation. I.U.R. is supported by the Carnegie Institution of Washington through the Carnegie Observatories Fellowship. J.E.L. acknowledges support from NASA Grant NNX10AN93G.

Facilities: HST (STIS), ESO:3.6m (HARPS), VLT:Kueyen (UVES), Keck:I (HIRES)

REFERENCES

- Akerman, C. J., Carigi, L., Nissen, P. E., Pettini, M., & Asplund, M. 2004, *A&A*, 414, 931
- Ahmad, S. A., Rao, P. M., & Afzal, S. M. 1997, *Zeitschrift fur Physik D Atoms Molecules Clusters*, 42, 165
- Aldenius, M., Lundberg, H., & Blackwell-Whitehead, R. 2009, *A&A*, 502, 989
- Aller, L. H., & Greenstein, J. L. 1960, *ApJS*, 5, 139
- Arlandini, C., Käppeler, F., Wisshak, K., et al. 1999, *ApJ*, 525, 886
- Asplund, M., Lambert, D. L., Nissen, P. E., Primas, F., & Smith, V. V. 2006, *ApJ*, 644, 229
- Asplund, M., Grevesse, N., Sauval, A. J., & Scott, P. 2009, *ARA&A*, 47, 481
- Ayres, T. R. 2010, *ApJS*, 187, 149
- Barbuy, B., Spite, M., Hill, V., et al. 2011, *A&A*, 534, A60
- Baruah, S., Audi, G., Blaum, K., et al. 2008, *Physical Review Letters*, 101, 262501
- Bengtsson, G. J., Berzinsh, U., Larsson, J., & Svanberg, S. 1992a, *A&A*, 263, 440
- Bengtsson, G. J., Berzinsh, U., Larsson, J., & Svanberg, S. 1992b, *Zeitschrift fur Physik D Atoms Molecules Clusters*, 23, 29
- Bengtsson, G. J., Berzinsh, U., Larsson, J., Svanberg, S., & Zerne, R. 1992c, *Journal de Physique II*, 2, 773
- Bergemann, M., & Cescutti, G. 2010, *A&A*, 522, A9
- Bergeson, S. D., & Lawler, J. E. 1993, *ApJ*, 408, 382
- Berkeland, D. J., Miller, J. D., Bergquist, J. C., Itano, W. M., & Wineland, D. J. 1998, *Physical Review Letters*, 80, 2089
- Bessell, M. S., & Norris, J. 1982, *ApJ*, 263, L29
- Bielski, A. 1975, *J. Quant. Spec. Radiat. Transf.*, 15, 463
- Biémont, E., Grevesse, N., Faires, L. M., et al. 1989, *A&A*, 209, 391
- Biémont, E., Dutriex, J.-F., Martin, I., & Quinet, P. 1998, *Journal of Physics B Atomic Molecular Physics*, 31, 3321
- Biémont, E., Garnir, H. P., Palmeri, P., Li, Z. S., & Svanberg, S. 2000, *MNRAS*, 312, 116
- Biémont, É., Blagoev, K., Engström, L., et al. 2011, *MNRAS*, 414, 3350
- Bieron, J. R., & Migdaek, J. 1992, *Journal of Physics B Atomic Molecular Physics*, 25, 4099
- Bisterzo, S., Gallino, R., Straniero, O., Cristallo, S., & Käppeler, F. 2011, *MNRAS*, 418, 284
- Blackwell, D. E., Petford, A. D., Shallis, M. J., & Leggett, S. 1982a, *MNRAS*, 199, 21
- Blackwell, D. E., Menon, S. L. R., Petford, A. D., & Shallis, M. J. 1982b, *MNRAS*, 201, 611
- Blackwell, D. E., Booth, A. J., Petford, A. D., & Laming, J. M. 1989, *MNRAS*, 236, 235
- Blagoev, K. B., Malcheva, G., Penchev, V., et al. 2004, *Phys. Scr.*, 69, 433
- Blaise, J., Vergés, J., Wyart, J.-F., & Engleman, R., Jr. 1992, *Journal de Physique II*, 2, 947
- Blum, R. D., & McGregor, P. J. 2008, *AJ*, 135, 1708
- Boesgaard, A. M., Rich, J. A., Levesque, E. M., & Bowler, B. P. 2011, *ApJ*, 743, 140
- Böhlke, J. K., de Laeter, J. R., De Bièvre, P., et al. 2005, *Journal of Physical and Chemical Reference Data*, 34, 57
- Bouazza, S., Guern, Y., Abjean, R., & Bauche, J. 1987, *Zeitschrift fur Physik D Atoms Molecules Clusters*, 7, 33
- Boyce, D. D., Barstow, M. A., Dobbie, P. D., et al. 2008, *ASP Conference Series*, "Hydrogen-Deficient Stars," Werner, K. & Rauch, T., eds. 391, 235
- Brage, T., Proffitt, C., & Leckrone, D. S. 1999, *ApJ*, 513, 524
- Brimicombe, M. S. W. M., Stacey, D. N., Stacey, V., Hühnermann, H., & Menzel, N. 1976, *Proc. R. Soc. Lond. A*, 352, 141
- Brown, M. S., Federman, S. R., Irving, R. E., Cheng, S., & Curtis, L. J. 2009, *ApJ*, 702, 880
- Burns, K., & Adams, K. B. 1956, *Journal of the Optical Society of America* (1917-1983), 46, 94
- Burt, E. A., Taghavi-Larigani, S., & Tjoelker, R. L. 2009, *Phys. Rev. A*, 79, 062506
- Caffau, E., Bonifacio, P., Faraggiana, R., et al. 2005, *A&A*, 441, 533
- Cameron, A. G. W. 1982, *Ap&SS*, 82, 123
- Cardelli, J. A., Federman, S. R., Lambert, D. L., & Theodosiou, C. E. 1993, *ApJ*, 416, L41
- Cardon, B. L., Smith, P. L., Scalo, J. M., Testerman, L., & Whaling, W. 1982, *ApJ*, 260, 395
- Casdorf, R., Enders, V., Blatt, R., Neuhauser, W., & Toschek, P. E. 1991, *Ann. Physik*, 503, 41
- Castelli, F., & Kurucz, R. L. Proc. IAU Symp. No 210, *Modelling of Stellar Atmospheres*, N. Piskunov et al., eds. 2003, A20
- Chang, T. N., & Tang, X. 1990, *J. Quant. Spec. Radiat. Transf.*, 43, 207
- Chayer, P., Vennes, S., Dupuis, J., & Kruk, J. W. 2005, *ApJ*, 630, L169
- Chen, M. H., & Cheng, K. T. 2010, *Journal of Physics B Atomic Molecular Physics*, 43, 074019
- Chou, H.-S., Chi, H.-C., & Huang, K.-N. 1994, *Phys. Rev. A*, 49, 2394

- Cowan, J. J., Sneden, C., Truran, J. W., & Burris, D. L. 1996, *ApJ*, 460, L115
- Cowan, J. J., Sneden, C., Burles, S., et al. 2002, *ApJ*, 572, 861
- Cowan, J. J., Sneden, C., Beers, T. C., et al. 2005, *ApJ*, 627, 238
- Crespo López-Urrutia, J. R., Kenner, B., Neger, T., & Jäger, H. 1994, *J. Quant. Spec. Radiat. Transf.*, 52, 111
- Dekker, H., D'Odorico, S., Kaufer, A., Delabre, B., & Kotzłowski, H. 2000, *Proc. SPIE*, 4008, 534
- de Medeiros, J. R., Silva, J. R. P., Do Nascimento, J. D., Jr., et al. 2006, *A&A*, 458, 895
- Den Hartog, E. A., Lawler, J. E., Sneden, C., & Cowan, J. J. 2003, *ApJS*, 148, 543
- Den Hartog, E. A., Herd, M. T., Lawler, J. E., et al. 2005, *ApJ*, 619, 639
- Den Hartog, E. A., Lawler, J. E., Sneden, C., & Cowan, J. J. 2006, *ApJS*, 167, 292
- Den Hartog, E. A., Lawler, J. E., Sobeck, J. S., Sneden, C., & Cowan, J. J. 2011, *ApJS*, 194, 35
- Dillmann, I., Kratz, K.-L., Wöhr, A., et al. 2003, *Physical Review Letters*, 91, 162503
- Dinerstein, H. L. 2001, *ApJ*, 550, L223
- Dixit, G., Nataraj, H. S., Sahoo, B. K., Chaudhuri, R. K., & Majumder, S. 2008a, *Journal of Physics B Atomic Molecular Physics*, 41, 025001
- Dixit, G., Nataraj, H. S., Sahoo, B. K., Chaudhuri, R. K., & Majumder, S. 2008b, *Phys. Rev. A*, 77, 012718
- Doerr, A., Kock, M., Kwiatkowski, M., & Werner, K. 1985, *J. Quant. Spec. Radiat. Transf.*, 33, 55
- Donnelly, D., Hibbert, A., & Bell, K. L. 1999, *Phys. Scr*, 59, 32
- Dworetsky, M. M. 1969, *ApJ*, 156, L101
- Elbel, M., Fischer, W., & Hartmann, M. 1963, *Zeitschrift für Physik*, 176, 288
- Elbel, M. & Hühnermann, H. 1969, *J. Phys. (Paris) Colloques*, 30, C1-41
- Farouqi, K., Kratz, K.-L., Mashonkina, L. I., et al. 2009, *ApJ*, 694, L49
- Farouqi, K., Kratz, K.-L., Pfeiffer, B., et al. 2010, *ApJ*, 712, 1359
- Fuhr, J. R. & Wiese, W. L. 2009, *Atomic Transition Probabilities*, published in the CRC Handbook of Chemistry and Physics, 90th Edition, Lide, D. R., ed. CRC Press, Inc., Boca Raton, FL
- Fulbright, J. P. 2002, *AJ*, 123, 404
- Głowacki, L., & Migdalek, J. 2009, *Phys. Rev. A*, 80, 042505
- Gratton, R. G., & Sneden, C. 1991, *A&A*, 241, 501
- Gratton, R. G., Sneden, C., Carretta, E., & Bragaglia, A. 2000, *A&A*, 354, 169
- Grevesse, N., Blackwell, D. E., & Petford, A. D. 1989, *A&A*, 208, 157
- Guern, Y., Bideau-Méhu, A., Abjean, R., & Johannin-Gilles, A. 1977, *Physica Scripta*, 14, 273
- Gullberg, D., & Litzén, U. 2000, *Phys. Scr*, 61, 652
- Hannaford, P., & Lowe, R. M. 1983, *Journal of Physics B Atomic Molecular Physics*, 16, 4539
- Hansen, C. J., & Primas, F. 2011, *A&A*, 525, L5
- Hansen, C. J., et al. 2012, *A&A*, submitted
- Harrison, S. A., & Hibbert, A. 2003, *MNRAS*, 340, 1279
- Holmberg, J., Nordström, B., & Andersen, J. 2007, *A&A*, 475, 519
- Holmgren, L. 1975, *Phys. Scr*, 11, 15
- Honda, S., Aoki, W., Ishimaru, Y., Wanajo, S., & Ryan, S. G. 2006, *ApJ*, 643, 1180
- Howard, L. E., & Andrew, K. L. 1985, *Journal of the Optical Society of America B Optical Physics*, 2, 1032
- Israelian, G., Ecuivillon, A., Rebolo, R., et al. 2004, *A&A*, 421, 649
- Ivans, I. I., Simmerer, J., Sneden, C., et al. 2006, *ApJ*, 645, 613
- Ivarsson, S., Wahlgren, G. M., Dai, Z., Lundberg, H., & Leckrone, D. S. 2004, *A&A*, 425, 353
- Jelenković, B. M., Chung, S., Prestage, J. D., & Maleki, L. 2006, *Phys. Rev. A*, 74, 022505
- Johnson, J. A., & Bolte, M. 2002, *ApJ*, 579, 616
- Johnson, J. A., Herwig, F., Beers, T. C., & Christlieb, N. 2007, *ApJ*, 658, 1203
- Jonsell, K., Edvardsson, B., Gustafsson, B., et al. 2005, *A&A*, 440, 321
- Käppeler, F., Beer, H., & Wisshak, K. 1989, *Rep. Prog. Phys.*, 52, 945
- Kedzierski, D., Kusz, J., & Muzolf, J. 2010, *Spectrochimica Acta B*, 65, 248
- Kerkhoff, H., Schmidt, M., & Zimmermann, P. 1980, *Zeitschrift für Physik A Atoms and Nuclei*, 298, 249
- Kimble, R. A., Woodgate, B. E., Bowers, C. W., et al. 1998, *ApJ*, 492, L83
- Kono, A., & Hattori, S. 1982, *Journal of the Optical Society of America (1917-1983)*, 72, 601
- Kratz, K.-L., Bitouzet, J.-P., Thielemann, F.-K., Moeller, P., & Pfeiffer, B. 1993, *ApJ*, 403, 216
- Kratz, K.-L., Farouqi, K., Pfeiffer, B., et al. 2007, *ApJ*, 662, 39
- Kurucz, R. L., & Bell, B. 1995, *Kurucz CD-ROM*, Cambridge, MA: Smithsonian Astrophysical Observatory
- Laird, J. B. 1985, *ApJ*, 289, 556
- Lawler, J. E., & Dakin, J. T. 1989, *Journal of the Optical Society of America B Optical Physics*, 6, 1457
- Lawler, J. E., Bonvallet, G., & Sneden, C. 2001a, *ApJ*, 556, 452
- Lawler, J. E., Wickliffe, M. E., Den Hartog, E. A., & Sneden, C. 2001b, *ApJ*, 563, 1075
- Lawler, J. E., Den Hartog, E. A., Sneden, C., & Cowan, J. J. 2006, *ApJS*, 162, 227
- Lawler, J. E., Sneden, C., Cowan, J. J., Wyart, J.-F., Ivans, I. I., Sobeck, J. S., Stockett, M. H., & Den Hartog, E. A. 2008, *ApJS*, 178, 71
- Lawler, J. E., Sneden, C., Cowan, J. J., Ivans, I. I., & Den Hartog, E. A. 2009, *ApJS*, 182, 51
- Leckrone, D. S., Wahlgren, G. M., & Johansson, S. G. 1991, *ApJ*, 377, L37
- Leckrone, D. S., Proffitt, C. R., Wahlgren, G. M., Johansson, S. G., & Brage, T. 1999, *AJ*, 117, 1454
- Lindgren, B., & Palenius, H. P. 1977, *Sol. Phys.*, 53, 347
- Liu, Y., Hutton, R., Zou, Y., Andersson, M., & Brage, T. 2006, *Journal of Physics B Atomic Molecular Physics*, 39, 3147
- Ljung, G., Nilsson, H., Asplund, M., & Johansson, S. 2006, *A&A*, 456, 1181
- Lotrian, J., Guern, Y., & Cariou, J. 1980, *Journal of Physics B Atomic Molecular Physics*, 13, 685
- Lotrian, J., & Guern, Y. 1982, *Journal of Physics B Atomic Molecular Physics*, 15, 69
- Lundberg, H., Engström, L., Hartman, H., et al. 2010, *Journal of Physics B Atomic Molecular Physics*, 43, 085004
- Malcheva, G., Blagoev, K., Mayo, R., et al. 2006, *MNRAS*, 367, 754
- Martin, W. C., Zalubas, R., & Hagan, L. 1978, *Atomic Energy Levels The Rare Earth Elements*, NSRDS-NBS 60 (Washington, DC: US Govt Printing Office)
- Mashonkina, L., & Gehren, T. 2001, *A&A*, 376, 232
- Mashonkina, L., Gehren, T., Shi, J.-R., Korn, A. J., & Grupp, F. 2011, *A&A*, 528, A87
- Mashonkina, L., Ryabtsev, A., Frebel, A. 2012, *A&A*, in press (arXiv:1202.2630)
- Mayor, M., Pepe, F., Queloz, D., et al. 2003, *The Messenger*, 114, 20
- McWilliam, A. 1998, *AJ*, 115, 1640
- Meléndez, J., & Barbuy, B. 2009, *A&A*, 497, 611
- Merrill, P. W. 1926, *ApJ*, 63, 13
- Moehring, D. L., Blinov, B. B., Gidley, D. W., et al. 2006, *Phys. Rev. A*, 73, 023413
- Molaro, P., Bonifacio, P., Castelli, F., & Pasquini, L. 1997, *A&A*, 319, 593
- Morgan, W. W. 1933, *ApJ*, 77, 77
- Morillon, C., & Vergès, J. 1974, *Phys. Scr*, 10, 227
- Morton, D. C. 2000, *ApJS*, 130, 403
- Münch, A., Berkler, M., Gerz, Ch., Wilsdorf, D., & Werth, G. 1987, *Phys. Rev. A*, 35, 4147
- Nilsson, H., & Pickering, J. C. 2003, *Phys. Scr*, 67, 223
- Nilsson, H., Ljung, G., Lundberg, H., & Nielsen, K. E. 2006, *A&A*, 445, 1165
- Nissen, P. E., Primas, F., Asplund, M., & Lambert, D. L. 2002, *A&A*, 390, 235
- Nissen, P. E., Akerman, C., Asplund, M., et al. 2007, *A&A*, 469, 319
- Nitz, D. E., Kunau, A. E., Wilson, K. L., & Lentz, L. R. 1999, *ApJS*, 122, 557
- O'Brian, T. R., Wickliffe, M. E., Lawler, J. E., Whaling, W., & Brault, J. W. 1991, *J. Opt. Soc. Am. B Optical Physics*, 8, 1185
- Parkinson, W. H., Reeves, E. M., & Tomkins, F. S. 1976, *Journal of Physics B Atomic Molecular Physics*, 9, 157

- Peck, E. R., & Reeder, K. 1972, *Journal of the Optical Society of America* (1917-1983), 62, 958
- Pendlebury, J. M., & Smith, K. F. 1964, *Proceedings of the Physical Society*, 84, 849
- Peterson, R. C. 2011, *ApJ*, 742, 21
- Pickering, J. C., Thorne, A. P., Murray, J. E., et al. 2000, *MNRAS*, 319, 163
- Pickering, J. C., Thorne, A. P., & Perez, R. 2001, *ApJS*, 132, 403
- Pickering, J. C., Thorne, A. P., & Perez, R. 2002, *ApJS*, 138, 247
- Pilachowski, C. A., Sneden, C., & Kraft, R. P. 1996, *AJ*, 111, 1689
- Pinnington, E. H., Ansbacher, W., Kernahan, J. A., Ahmad, T., & Ge, Z.-Q. 1988, *Canadian Journal of Physics*, 66, 960
- Pinnington, E. H., Berends, R. W., & Ji, Q. 1994, *Phys. Rev. A*, 50, 2758
- Pinnington, E. H., Rieger, G., Kernahan, J. A., & Biémont, E. 1997, *Canadian Journal of Physics*, 75, 1
- Primas, F., Duncan, D. K., & Thorburn, J. A. 1998, *ApJ*, 506, L51
- Primas, F., & Sobeck, J. 2008, *Evolution and Nucleosynthesis in AGB Stars*, R. Guandalini, S. Palmerini, & M. Busso, eds., 1001, 230
- Ralchenko, Yu., Kramida, A., Reader, J., et al. 2011, *NIST Atomic Spectra Database*, version 4.1, available online: <http://physics.nist.gov/asd>
- Reader, J., Meissner, K. W., & Andrew, K. L. 1960, *Journal of the Optical Society of America* (1917-1983), 50, 221
- Reader, J., Corliss, C. H., Wiese, W. L., & Martin, G. A. 1980, *Wavelengths and transition probabilities for atoms and atomic ions*, NSRDS-NBS 68 (Washington, DC: US Govt Printing Office)
- Roederer, I. U., Lawler, J. E., Sneden, C., et al. 2008, *ApJ*, 675, 723
- Roederer, I. U., Kratz, K.-L., Frebel, A., et al. 2009, *ApJ*, 698, 1963
- Roederer, I. U., Sneden, C., Lawler, J. E., & Cowan, J. J. 2010a, *ApJ*, 714, L123
- Roederer, I. U., Cowan, J. J., Karakas, A. I., et al. 2010b, *ApJ*, 724, 975
- Roederer, I. U., Lawler, J. E., Cowan, J. J., et al. 2012a, *ApJ*, 747, L8
- Roederer, I. U., Lawler, J. E., Sobeck, J. S., et al. 2012b, *ApJS*, submitted
- Roman-Lopes, A., Abraham, Z., Ortiz, R., & Rodriguez-Ardila, A. 2009, *MNRAS*, 394, 467
- Safronova, U. I., & Johnson, W. R. 2004, *Phys. Rev. A*, 69, 052511
- Sansonetti, C. J., & Reader, J. 2001, *Phys. Scr*, 63, 219
- Schlegel, D. J., Finkbeiner, D. P., & Davis, M. 1998, *ApJ*, 500, 525
- Schuttevaer, J. W., & Smit, J. A. 1943, *Physica*, 10, 502
- Seeger, P. A., Fowler, W. A., & Clayton, D. D. 1965, *ApJS*, 11, 121
- Sikström, C. M., Pihlmark, H., Nilsson, H., et al. 2001, *Journal of Physics B Atomic Molecular Physics*, 34, 477
- Simmons, M., Safronova, U. I., & Safronova, M. S. 2011, *Phys. Rev. A*, 84, 052510
- Sneden, C. A. 1973, Ph.D. Thesis, Univ. of Texas at Austin
- Sneden, C., Cowan, J. J., Burris, D. L., & Truran, J. W. 1998, *ApJ*, 496, 235
- Sneden, C., Cowan, J. J., Ivans, I. I., et al. 2000, *ApJ*, 533, L139
- Sneden, C., Cowan, J. J., Lawler, J. E., et al. 2003, *ApJ*, 591, 936
- Sneden, C., Cowan, J. J., & Gallino, R. 2008, *ARA&A*, 46, 241
- Sneden, C., Lawler, J. E., Cowan, J. J., Ivans, I. I., & Den Hartog, E. A. 2009, *ApJS*, 182, 80
- Sobeck, J. S., Ivans, I. I., Simmerer, J. A., et al. 2006, *AJ*, 131, 2949
- Sobeck, J. S., Lawler, J. E., & Sneden, C. 2007, *ApJ*, 667, 1267
- Sobeck, J. S., Kraft, R. P., Sneden, C., et al. 2011, *AJ*, 141, 175
- Spence, P. W., & McDermott, M. N. 1972, *Physics Letters A*, 42, 273
- St. John, C. E., & Moore, C. E. 1928, *ApJ*, 68, 93
- Sterling, N. C., & Dinerstein, H. L. 2008, *ApJS*, 174, 158
- Sugar, J., & Musgrove, A. 1990, *Journal of Physical and Chemical Reference Data*, 19, 527
- Tan, K. F., Shi, J. R., & Zhao, G. 2009, *MNRAS*, 392, 205
- Theodosiou, C. E. 1986, *Journal of the Optical Society of America B Optical Physics*, 3, 1107
- Theodosiou, T., Griffith, J. A. R., Cooke, J. L., & Forest, D. H. 1997, *Journal of Physics B Atomic Molecular Physics*, 30, L635
- Thévenin, F., & Idiart, T. P. 1999, *ApJ*, 521, 753
- Tomkin, J., Lemke, M., Lambert, D. L., & Sneden, C. 1992, *AJ*, 104, 1568
- Travaglio, C., Gallino, R., Arnone, E., et al. 2004, *ApJ*, 601, 864
- Ubelis, A. P., & Berzinsh, U. V. 1986, *Phys. Scr*, 34, 805
- Unsöld, A., *Physik der Sternatmosphären*, Springer-Verlag, Berlin, 1955, p. 332
- van Leeuwen, F. 2007, *A&A*, 474, 653
- Van Eck, S., Goriely, S., Jorissen, A., & Plez, B. 2001, *Nature*, 412, 793
- Vogt, S. S., Allen, S. L., Bigelow, B. C., et al. 1994, *Proc. SPIE*, 2198, 362
- Wallerstein, G., Greenstein, J. L., Parker, R., Helfer, H. L., & Aller, L. H. 1963, *ApJ*, 137, 280
- Wanajo, S., Janka, H.-T., Müller, B. 2011, *ApJ*, 726, L15
- Weiss, A. W. 1995, *Phys. Rev. A*, 51, 1067
- Whaling, W., & Brault, J. W. 1988, *Phys. Scr*, 38, 707
- Wickliffe, M. E., Salih, S., & Lawler, J. E. 1994, *J. Quant. Spec. Radiat. Transf.*, 51, 545
- Wickliffe, M. E., Lawler, J. E., & Nave, G. 2000, *J. Quant. Spectr. Radiat. Trans.*, 66, 363
- Woodgate, B. E., Kimble, R. A., Bowers, C. W., et al. 1998, *PASP*, 110, 1183
- Woosley, S. E., & Hoffman, R. D. 1992, *ApJ*, 395, 202
- Xu, H. L., Sun, Z. W., Dai, Z. W., et al. 2006, *A&A*, 452, 357
- Zhao, G., & Magain, P. 1990, *A&A*, 238, 242